The impact of high magnitude precipitation events and sediment availability on the occurrence of debris floods in the Gratzental basin, Austria.

Master's Thesis

Faculty of Science

University of Bern

presented by

Jérôme Wider

2011

Supervisor:

Prof. Dr. Fritz Schlunegger

Institute of Geological Sciences and Oeschger Centre for Climate Change Research

Co-Supervisor:

Prof. Dr. Jürg Luterbacher

Chair for Climatology, Climate Dynamics and Climate Change, Department of Geography, Justus-Liebig University Giessen, Germany, and Oeschger Centre for Climate Change Research

Advisor:

Dr. Markus Stoffel

Institute of Geological Sciences and Oeschger Centre for Climate Change Research

Abstract

Debris flows are a global hazardous phenomenon with a very high damage potential. Mainly triggered by extreme rainfall events, debris flows are sensitive to changes in precipitation patterns. Whereas changes in the occurrence of extreme rainfall events are partly observable in the station records, the sensitivity of the triggering of debris flows on the precipitation characteristics remains unclear for most debris flow catchments.

Thus in this work we perform a sensitivity analysis of a transport-limited debris flood catchment in Tirol, Austria. To this end, multiple sources of data are combined in a semi-empirical approach that makes use of field survey methods, geomorphic techniques, statistics and synoptical climatology for a detailed reconstruction of past debris flood activity. Seasonality of the debris floods, triggering rainfall thresholds and large-scale 500hPa geopotential height field anomalies related to extreme precipitation events and the occurrence of debris floods in this catchment are discussed.

Even if this first approach offers several possibilities for further improvement, it seems promising to establish the link between atmospherical anomalies and extreme rainfalls to the triggering of debris floods with data that is readily available around the globe.

Table of Contents

List of figures

List of tables

1 Introduction

1.1 General context

Gravity-induced mass movements are very prominent in mountain environments and often pose a threat to infrastructure and the population living at the foot of the mountains. Debris flows are among the most frequent and most effective mass-movement processes and occur in steep slopes everywhere around the globe. Due to the fact that debris flows reach very high velocities and that the temporal predictability of their occurrence still is very poor, they are commonly regarded as one of the most dangerous and destructive landslide types *(Jakob and Hungr, 2005)*.

Most landslides and debris flows are generated during heavy rainstorms through the rapid infiltration of prolonged intense rainfalls. The infiltration leads to the water saturation of the soil and a temporary increase in pore-water pressure. High pore-water pressures destabilize the soil and thus reduce its shear strength *(Caine, 1980; Iverson, 2000; Wieczorek and Glade, 2005)*.

Extreme rainfall events, characterized by large magnitudes and high intensities, are expected to react more directly to a rise in atmospheric moisture content than normal rainfall events. The current rise in atmospheric moisture content is a consequence of the warming of the atmosphere due to increased greenhouse gas concentrations *(Frei et al., 1998; Trenberth, 1999; Frei et al., 2000)*. Simulations of atmospheric warming with global climate models (GCM) suggest an intensification of the hydrological cycle. Per degree heating, an increase of the atmospheric moisture content of 7% was calculated *(Delgenio et al., 1991)*. Regional climate models (RCM) have revealed attendant effects upon the

frequency of strong precipitation events. *Frei et al. (1998)* detected with RCM simulations a substantial shift towards a higher frequency of strong precipitation events over Europe and for the fall season.

On the global scale, widespread increases in heavy precipitation events have already been observed, even at places where total rainfall amounts have decreased *(Trenberth et al., 2007)*. On the scale of the Alpine countries, trends of an increasing frequency of strong precipitation events are observable as well. Significant changes in the occurrence of strong precipitation events in Switzerland were reported for autumn and winter *(Schmidli and Frei, 2005)*. However, extremes are by definition events that occur very rarely. There exist strong limitations for the detectability of trends for extremes in time series of past observations. In fact, using time series that span an entire century, trend analysis is restricted to rainfall events that have return periods below 30 days, while trends of stronger event classes are not detectable with statistical significance *(Frei et al., 2000; Frei and Schar, 2001)*.

The sensitivity of debris flows to a change in climate parameters has been analyzed by several studies. In the Swiss Alps, *Stoffel and Beniston (2006)* found significant changes in the seasonality of past debris flows related to a change in the occurrence of heavy rainfall events. *Jomelli et al. (2007)* and *Jomelli et al.(2004)* found in their studies in the French Alps that the response of hill slope debris flows to climatic change is strongly dependent on the type of debris flow.

Even if the relation between heavy rainfall and the triggering of shallow landslides and debris flows is obvious, it is difficult to describe precisely, as rainfall influences soil stability only indirectly through its effect on pore water conditions in slope material *(Caine, 1980)*.

1.2 Thesis' research focus

The main focus of this study was on

i) Assessing the sensitivity of a specific debris-flood system to hydroclimatic events. The aim of this assessment is to establish the link between the geomorphic catchment characteristics and the triggering of debris floods through strong precipitation events.

ii) Using different archives to characterize well known past events in order to increase the temporal resolution of further past debris flood events at the study site.

iii) Enhancing the use of station rainfall data from regular networks in the context of debris-flood triggering. This is done by the use of multiple station records in combination with statistical methods. The possibility of a derivation of reasonable thresholds for the triggering of debris floods in the catchment is also examined. Additionally, the station records are analyzed in regard of trends and return levels of extreme precipitation events.

iv) Linking the debris-flood events with associated large-scale atmospheric circulation patterns. Thereby the large-scale weather situations that preferably lead to debris floods at the study site are identified.

1.3 State of research

In debris-flow studies, the knowledge of event frequency and magnitude provides a rational basis for both hazard zonation and the design of mitigation structures *(Bovis and Jakob, 1999)*. However, there are still difficulties to account for processes with a very low frequency or a high recurrence time. As the debris flows occur very infrequent, a year-round, fully equipped surveillance is not

practicable or at least does not seem very feasible. Thereof results a lack of data concerning the event frequency and triggering factors of debris flows. This imposes significant difficulties to frequency-magnitude analyses *(Strunk, 1995)*. Dendrogeomorphic reconstructions of past events have proven a valuable tool to fill this gap *(Stoffel, 2007; Stoffel and Bollschweiler, 2008; Mayer et al., 2010; Stoffel, 2010)*.

Up to date, a number of studies have been conducted on intensity-duration thresholds for the triggering of landslides and debris flows at different locations and on different spatial scales *(e.g. (Caine, 1980; De Vita et al., 1998; Guzzetti et al., 2007; Guzzetti et al., 2008)*. An important issue in the inference of these thresholds is the quality (temporal resolution) of rainfall data. Several authors *(e.g.: Strunk, 1995; Deganutti et al., 2000*) stated that daily rainfall data from standard rain gauge networks are suitable for regional analyses of storms and rainfalls but not at the local scale. Accordingly, only hourly rainfall totals from experimental weather stations are capable of establishing the link between precipitation and debris flows.

Nevertheless, the global occurrence of debris flows points to the need to establish this link with little available data, as only few sites are established with experimental stations. A promising approach with high coverage is the use of rainfall data obtained through remote sensing. Up to date, however, the capabilities of radar and satellite remote sensing are still limited for the spatial resolution of smaller catchments and need accurate ground-based verification *(Wieczorek et al., 2003)*.

Consequently, in this study we tried to account for these needs by applying statistical methods to define thresholds from the regular station network records.

A common problem with local triggering thresholds is that their transferability to other catchments is highly limited. This is due to specific catchment

characteristics such as morphologic, lithologic as well as meteorological and climatic differences, whereas the latter are normally not accounted for in the formation of local thresholds *(Guzzetti et al., 2007)*. In this study, the climatic factors are explicitly included in the analysis of the catchment to increase the transferability of the results to other catchments.

In general, two different model types are used to generate rainfall thresholds for the triggering of landslides and debris flows: Process-based and empirically based models. The first model type is based on detailed representations of the physical processes that occur during the triggering of a debris flow. The second model type is based on statistical analyses and historical data of rainfall events that triggered landslides. Thresholds are usually obtained by drawing lower-bound lines to the rainfall conditions that resulted in landslides, plotted in a coordinate system *(Guzzetti et al., 2007)*. There does not exist a unique set of measures to characterize rainfall events that led to the occurrence of landslides and debris flows, but a variety of different measures are described in the literature *(Guzzetti et al., 2007)*.

A different approach that lies in between physical and empirical models is provided by the antecedent soil water status model *(Crozier, 1999)*. The aim of this model is to provide a 24-hour forecast of landslide occurrence based on an index of soil water content and the forecasted precipitation amounts. Soil water status is used empirically to identify a threshold condition for the triggering of landslides.

The approach of this study is also semi-empirical. Long records of rain gauges were used in combination with GIS, historical data of past events, tree ring data and field survey methods. Thereby we attempt to assess the catchment's susceptibility to trigger debris floods prior to deriving the characteristics of precipitation events that triggered debris floods in the past. With the selection of a

catchment where the dominating process has been described as debris flood *(Mayer et al., 2010)* we apply the procedure on a class of debris-flow movements that is strongly bound to the presence of large amounts of water *(Hungr, 2005)*.

1.4 Motivation

The principal motivation for this thesis was to examine an environmental system whereupon climate has a strong influence. The strong impact of climate in mountainous regions and the consequences of changes of relevant climate parameters gave reason to link the two interesting fields of climate sciences and geomorphology in this study. The challenge was to establish this link on an empirical basis in a catchment that is not equipped with specific experimental instruments.

2 Study site

2.1 Geography and local climate

This study was performed in the Gratzental, a small, branched glacial valley located in the northeastern Austroalpine nappes, close to Lake Achensee northeast of Innsbruck (Tyrol, Austria). The catchment of the Gratzentalbach (outlined by the broken line in Figure 1) encompasses approximately 2.1km^2 and ranges from 2106m a.s.l. (Mondscheinspitze) to 1126m a.s.l. at the confluence with the Pletzachbach.

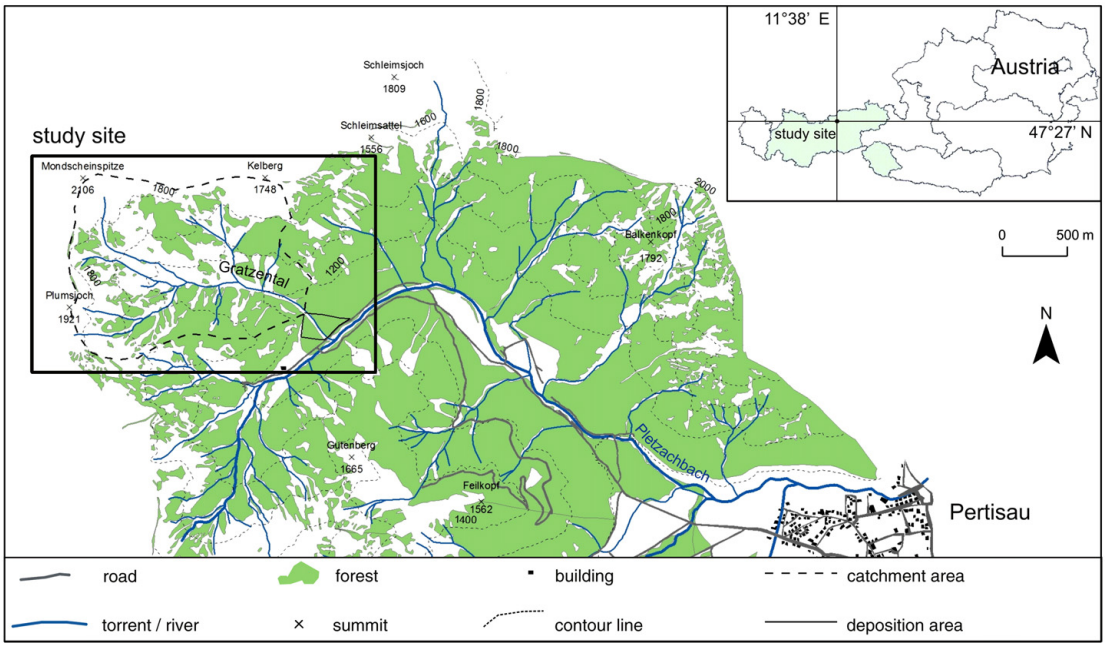

Figure 1: Location of the study site with the outline of the catchment of the Gratzentalbach *(Geol. Bundesanstalt, 2008; Mayer et al., 2010)*.

The geographical location of the study site implies a cool-humid climate, characterized by orographic blocking of northwesterly winds and frontal systems.

The site experiences relatively mild winters and temperate to cool humid summers. Annual precipitation amounts vary between 1300mm and 2500mm, with an annual mean of 1526mm (station Pertisau, 1895-2008). Approximately 57% of the precipitation amount falls between Mai and September, whereas the most intense precipitation events occur during July and August. Thunderstorms can deliver enormous precipitation amounts over short periods. The maximum value for a single precipitation event for the station Pertisau was recorded on 01.08.1992, when a severe thunderstorm yielded 74.6mm in 3-4 hours *(Hübl et al., 2002)*. At higher elevations in the catchment, orographic precipitation effects can significantly augment precipitation amounts.

The annual mean temperature for heights of 900-1000m a.s.l. is approximately 5.5 °C. At Pertisau, the coldest month is January (mean temperature -3.6 °C) and the highest monthly mean is registered in July (12.1 °C). According to Hübl et al. (2002), the area is covered by snow between mid December and mid April. Seasonal snow accumulations range from 6-9m and vary strongly due to local aspect and wind exposure.

2.2 Geological setting

The catchment is dominated by steep hillslopes of highly weathered and fractured grey or grey-brown dolomite (so called “Hauptdolomit”) of the Late Trias and local moraines *(Geol. Bundesanstalt, 2008)*. Figure 2 shows a general overview on the pattern of bedrock exposure.

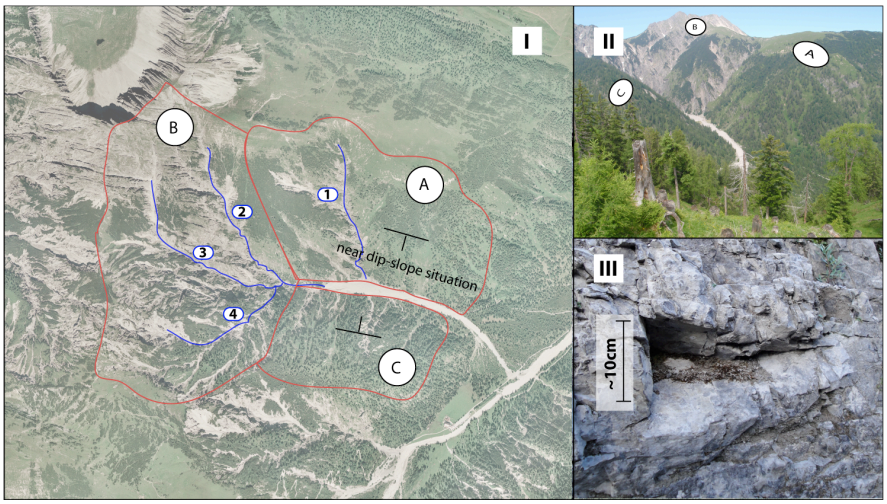

Figure 2: The Orthophoto (I) shows the different tributary catchments (A-C), the main tributary streams (1-4), the trunk stream (Gratzentalbach) and the bedding orientation. The upper photograph (II) is a view of the Gratzental, as seen from a hillslope on the opposite side. The lower photograph (III) was taken at the confluence of the streams 2, 3 and 4. It shows the highly fractured bedrock on the hillslopes directly above the channel.

The trunk channel of the Gratzental follows the southeast striking axial plane of the litho-tectonic units: North of the valley, the dolomite beds dip steeply (78°) towards southwest (210°; nearly dip-slope situation; tributary catchment A in Figure 2) whereas on the southern part (section C), the bedrock units dip isoclinally towards northeast. In contrast, on the western side of the catchment (section B), the bedrock dips in the opposite direction than the topographic slope.

The hillslopes above the channels expose highly fractured bedrock with a regolith cover several dm to m thick. The regolith easily breaks into pieces of ~1 dm^3.

3 Data

The study made use of different data sources. Figure 3 illustrates the temporal coverage of the datasets that were used in this study. Vertical lines represent the event-years reconstructed with dendrogeomorphic methods *(Mayer et al., 2010)*. Whereas most of the datasets have clearly defined temporal ranges, the coverage of the field survey observations is not defined.

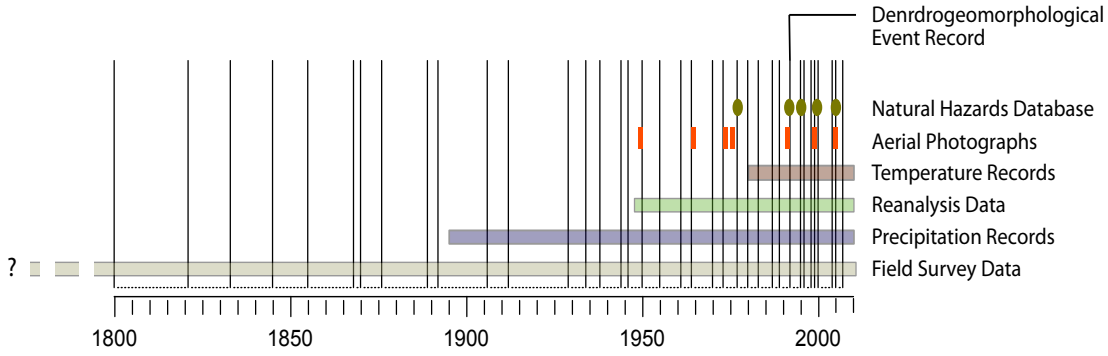

Figure 3: The figure shows the temporal coverage of the different datasets used in this study.

In the following, a short description of each dataset is given.

If debris floods affect trees, growth disturbances such as injuries, callus tissue, tangential rows of traumatic resin ducts, abrupt growth suppressions or releases or compression wood can be identified in the tree rings *(Stoffel and Bollschweiler, 2008)*. *Mayer et al. (2010)* analyzed 1155 growth disturbances from 227 trees, growing on the cone of the Gratzentalbach (deposition area in Figure 1), for a dendrogeomorphic reconstruction of past debris-flood activity. They were able to date 37 debris flood events that occurred between 1800 and 2007. This dataset was used as underlying basis for the reconstruction of past events.

Archival records of past flood and debris-flood events in the area were taken from an event-database of natural hazards in Tyrol (EDB) *(Forsttechn. Dienst für Wildbach- und Lawinenverbauung, 2009 a); Forsttechn. Dienst für Wildbach- und Lawinenverbauung, 2009 b))*. Five events therein matched event years from the dendrogeomorphic reconstruction. These events occurred in 1977, 1992, 1995, 1999 and 2005 and are hereafter referred to as EDB events.

A set of aerial photographs of the catchment was inspected to detect the most active regions regarding sediment supply. Photographs from the years 1952, 1964, 1973, 1974, 1992, 1998 and 2005 were used.

Daily temperature means for the stations Hinterriss, Rotholz, Schwaz and Weerberg were digitally available for the period 1981-2007.

Anomalies of 500hPa geopotential height were derived from NCEP/NCAR reanalysis data *(Kalnay, 1996)* for each day when an extreme precipitation event occurred. NCEP/NCAR reanalysis data is available for the time since 1948.

Another dataset employed in this study consisted of time series of daily precipitation totals. The records of 8 rain gauge stations surrounding the catchment were used. The stations were selected in order to give reasonable compromise between the length of the record period and the distance between gauging stations and the catchment. The first criterion is important for the significance of statistical measures (trends) whereas the second criterion accounts for the often very local occurrence of intense precipitation events.

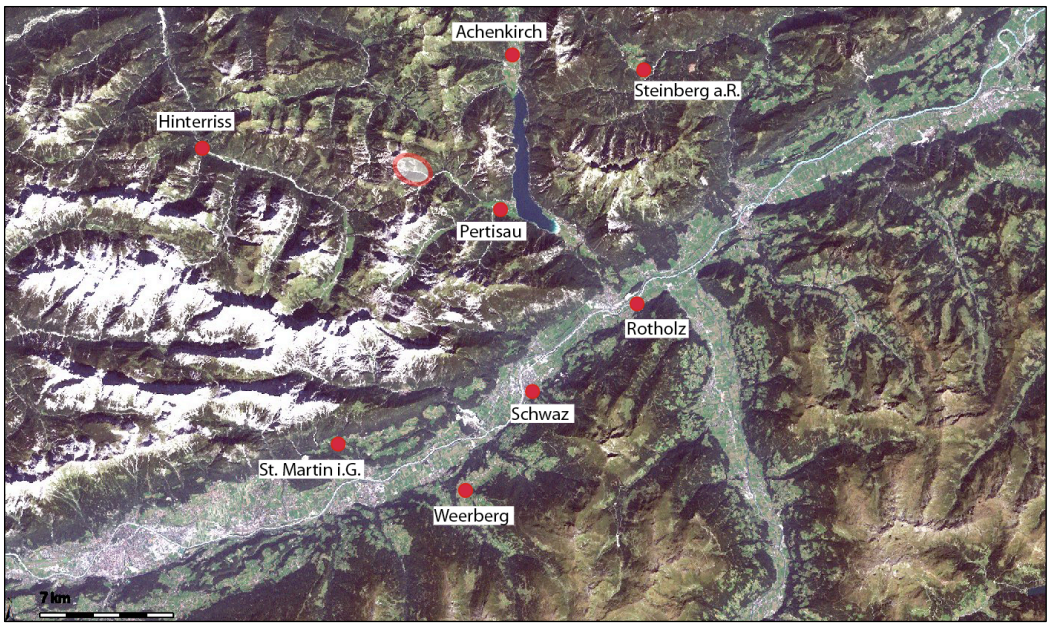

	Pertisau	Achenkirch	Hinterriss	Schwaz	Steinberg	Rotholz	St. Martin	Weerberg
Record period	1900-2007	1895-2007	1895-2008	1916-2008	1895-2008	1896-2008	1895-2008	1895-2008
Distance to catchment	5.5km	9.6km	12.5km	14km	14km	15km	16km	18.1km
Station height	935m	905m	930m	353m	1020m	590m	875m	925m

Figure 4: The map shows the rain gauges surrounding the catchment area. The red circle indicates the position of the study area. The table gives the properties of the rain gauge stations. Map from *(Land Tirol, 2010)*.

The stations chosen are at a maximum distance of 18.1 km to the catchment and at heights between 535m and 1020m a.s.l.. The longest precipitation records start in 1895 whereas the first measurements of the shortest record are from 1916. The station records contained several measurement gaps, but a minimum coverage of five stations was guaranteed for all event years. The tree-ring- and precipitation records show an overlap between 1895 and 2007, comprising 27 debris flood events.

Observations from the field delivered geological, geomorphic and sedimentological evidence for a characterization of the study area properties.

Additionally, a digital elevation model of the catchment with a vertical resolution of 1m was used for the analysis of channel profiles.

4 Methods

The approach of this study consists of three distinct steps. Each of these steps is dedicated a chapter. The first step (4.1) employs geomorphological methods and aims at the assessment of the catchment's susceptibility to trigger debris floods. This chapter will thereby provide an estimate on the size of the rainfall events that are capable of triggering debris floods in the study area. The next step (4.2) aims at a higher temporal resolution of past debris-flood events with statistical methods. Additionally, an improvement of the applicability of rainfall records from regular weather stations is searched in this context. This step provides the event-dates and the stations that will ultimately link the local extreme precipitation events with the associated atmospheric anomalies. This link to weather and climate patterns is established in chapter (4.3). The flowchart below illustrates the structure of the approach, the respective outputs and interlinkages of the individual analysis steps.

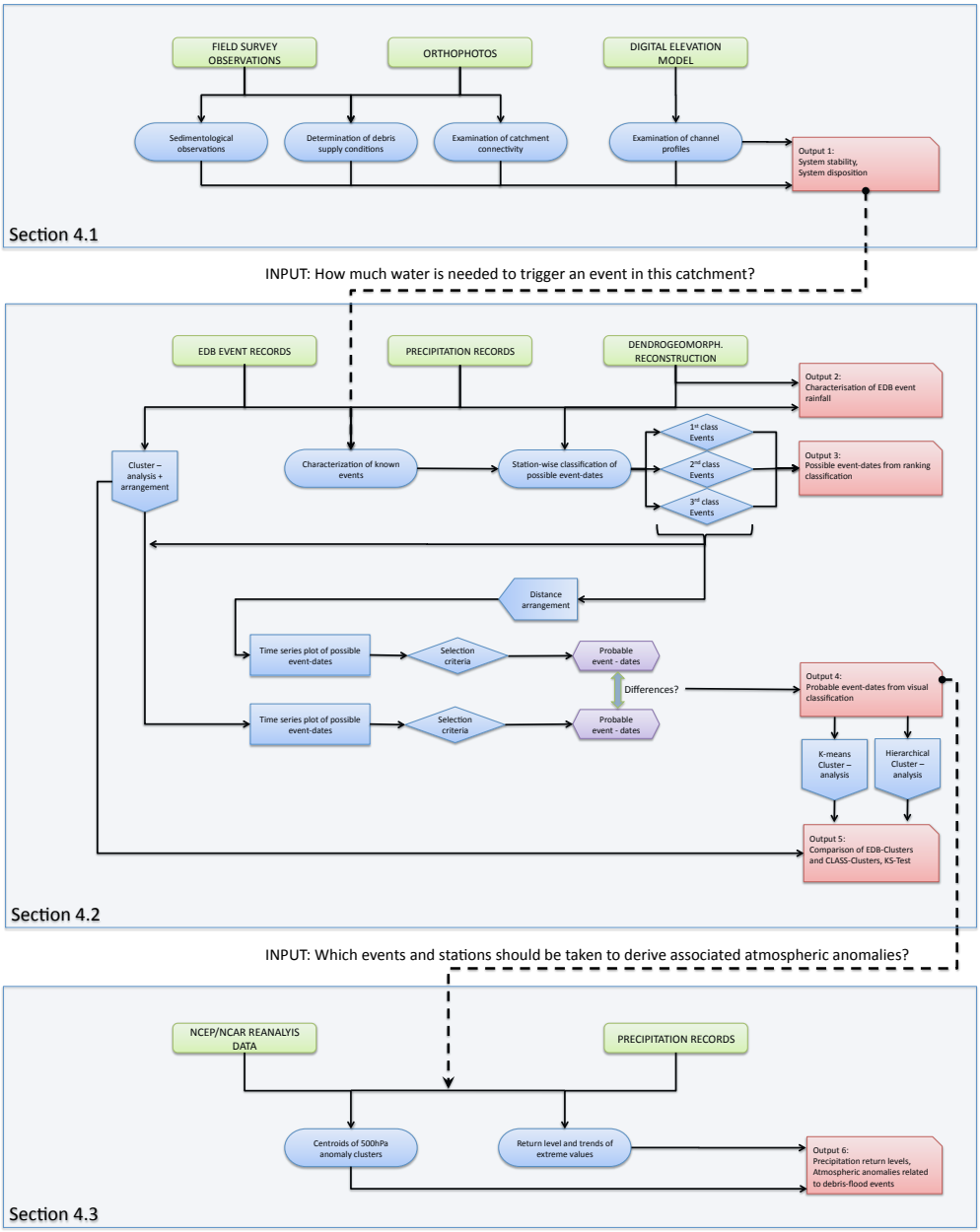

Figure 5: Flowchart showing the research structure of this study.

4.1 Assessment of the catchment's susceptibility for debris-flood generation

The susceptibility of the catchment for the triggering of debris floods is assessed in the following chapter. The aim is to integrate the geomorphic, sedimentologic and climatologic factors that contribute to the formation of a debris flood into a systematic concept. The application of the concept of disposition allows for a quantification of the relative importance of strong rainfall events on debris-flood triggering at the study area.

4.1.1 The concept of catchment disposition

Evidence from field observations in combination with results from GIS analysis and aerial photograph inspection are linked to strong precipitation events by means of the concept of catchment disposition originally described by *Kienholz (1995)*.

The term disposition refers to the susceptibility of a system to generate debris flows. There are two different types of disposition: The basic disposition and the variable disposition. Figure 6 illustrates the concept of disposition.

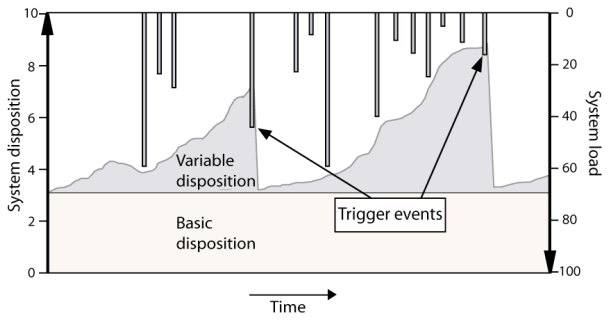

Figure 6: The concept of debris flow disposition. Note that only the combination of the system disposition and the magnitude of the trigger event make the generation of a debris-flood event possible. Redrawn after *Zimmermann (1997)*.

The basic disposition describes the general susceptibility of a system to generate debris flows. This susceptibility is mainly governed by the nature of the debris sources and their geotechnical properties as well as by the relief. Factors are constant over time or change over time scales from decades to centuries. The basic disposition determines the spatial occurrence of debris flows and their magnitude *(Zimmermann, 1997)*.

The variable disposition determines the short-term changes in susceptibility for debris-flow generation. These changes result from hydrometeorological variations at the scale of days to weeks as well as from debris supply conditions based on the torrent's history. These pre-event conditions change over weeks to years *(Zimmermann, 1997)*.

Besides the disposition, a system disturbance or system load in the form of a short-term impact is needed to generate a debris flow. This impact is called the trigger event. In the Alps, trigger-events are exclusively hydrological in nature. They are composed of either precipitation-dependent events like thunderstorms or long rainy periods. Or events that are independent of precipitation such as rapid melting of snow and ice as well as outbursts of glacial lakes *(Zimmermann, 1997)*.

In this study, basic and variable disposition were evaluated using evidence from channel profiles and geomorphic field observations. Thereof important indications for the size and character of the triggering rainfall events are inferred and consequently used in the analysis of the precipitation records.

4.1.2 Geomorphic properties

By means of a field survey and a GIS-analysis of channel profiles, the mechanisms of sediment transport in the study area and their fingerprints in the catchment are analyzed.

First, the basic geomorphic properties such as catchment topography and morphometry are recorded. Consecutively, the catchment is subdivided into three tributary catchments (A-C in Figure 1) with differing sediment transport activity. Differences in sediment transport activity are analyzed regarding a classification of the tributary basins as either transport- or supply- (weathering-) limited. This step is justified by a study of *(Bovis and Jakob, 1999)*, who argued that debris-flow magnitudes and frequency are functions of both hydroclimatic events as well as terrain variables, and that the sediment supply conditions in the more active basins are fundamental in predicting (and thus assessing) debris-flow activity *(Bovis and Jakob, 1999)*.

In transport-limited basins, an almost unlimited amount of sediment is available to feed debris flows. Thus debris-flow frequency in transport-limited basins is primarily controlled by hydroclimatic events, since the supply of mobilizeable sediment is rarely a limiting factor for debris-flow occurrence *(Bovis and Jakob, 1999)*. In supply-limited basins sediment supply and channel recharge rates are lower. Therefore a substantial time period must elapse before the next debris flow can occur and event frequency is generally lower in this type of basins *(Bovis and Jakob, 1999)*. The nature of the limitation of sediment discharge hence has important implications for potential threshold conditions for sediment transfer by debris flows and related mass wasting processes *(Schlunegger et al., 2009)*.

Transport-limited basins typically have a high density of headwater channels incised into thick glacial drift or closely jointed bedrock. Weathering- (supply-) limited basins show fewer zones of instability. This is usually due to a more massive bedrock or a thinner glacial drift *(Bovis and Jakob, 1999)*.

The classification was done based on aerial photographs. In accordance to *Bovis and Jakob (1999)*, the discrimination criteria were drainage density and debris

contributing area of the tributary catchments. Classification was done on the scale of the tributary basins as well as on the scale of the entire debris-flow system.

The next step focused on channel morphology. The longitudinal profiles of the four main tributary streams (1-4 in Figure 1) are examined. Spikes were removed form the plots and a smoothing filter with a 100m-window was applied. Consequently, sections dominated by gravity-driven- and fluvial processes were identified in the associated logarithmic plots of slope (S) against drainage area (A). This was done according to studies from *Flint (1974)*, who stated that the profile of a graded stream appears as a straight line with a constant negative slope in the log (S)-log (A) plots. Graded longitudinal stream profiles are considered to be in equilibrium in relation to environmental effects and sediment transport. Horizontal lines or lines with positive slopes on these plots indicate sections of gravity-driven processes, mainly found in the headwater reaches. Slightly negative slopes on plots indicate a dominance of fluvial processes, which mostly dominate the lower reaches of a channel. Steps in the logarithmic plots indicate transient zones regarding the dominant sediment transport mechanisms. A more comprehensive description of profile-plots and associated sediment transport processes is provided in the Appendix.

4.1.3 Sedimentological fabric

Another important objective of the field survey was the examination of the fabric of channel deposits at different sites. The aim was to document the mechanisms of sediment transfer in the catchment. Thus the documentation focused on the sorting, structure and grain size distribution of the sediment in channels and on debris fans. Observations concerning water seepage in the trunk channel were made as well.

4.2 Increasing the temporal resolution of debris-flood event records

The first part of the analysis of the rainfall data aimed at obtaining a more precise dating of the debris-flood events. The objective was to reach a daily resolution, i.e. to derive the exact dates when the debris floods occurred in the past.

For that purpose, the rainfall characteristics of known events (EDB dates) were recorded first. These characteristics served as a reference for the subsequent dating of further events that occurred in the past.

A stationwise classification of possible event dates was performed on the basis of the EDB event characteristics. This procedure is referred to as ranking classification of possible event-dates.

Seeking for structure in the rainfall data, cluster analysis was performed, arranging the weather stations into distinct groups.

In the following, the yearly time series of rainfall at event years were plotted together, whereas possible event-dates from the ranking classification were marked in the time series of each station. Taking into account the different event-classes from the ranking classification, either the accordance of possible events or the occurrence of a high event-class at specific stations was considered more important for the identification of a single date per year (CLASS date). This procedure is referred to as visual event-classification and was done twice. The first series of plots were produced with the stations arranged according to their distance from the catchment. In the second series, the stations were arranged according to the grouping obtained through cluster analysis.

The classification is evaluated by taking into account the event-rainfalls of all the classified event-dates (EDB and CLASS dates). Two types of cluster analysis are done to check whether the structure of the initial cluster analysis with EDB could

be reproduced. Additionally, a significance test is made on the means of the two groups with the null hypothesis of equal means in the two groups of event-rainfalls (EDB events vs. CLASS events).

4.2.1 Characterisation of event-date precipitation

Means and standard deviations of rainfall at EDB event dates and antecedent to the known events (up to a period of 5 days) were used to support the choice of the appropriate temporal aggregation of rainfall data for further analysis. Thus a choice of the significant rainfall period responsible for the triggering of debris floods in the catchment was made.

No assumptions on the spatial precipitation patterns of the triggering events were made at this point. Thus the characterization of the events was held elementary and only the three stations next to the catchment (Pertisau, Achenkirch, Hinterriss) were used.

4.2.2 Ranking classification of possible event-dates

With the characteristics of the triggering EDB events analyzed, a station-wise ranking classification of possible event dates during past event years (as obtained from dendrogeomorphic reconstruction) was performed.

Based on summary statistics of the station rainfall records, we identified three different event-classes: Class 1 events consisted of EDB dates. Class 2 events were those dates that were found within seasonal borders and whose daily rainfall amounts exceeded the second largest event by more than one standard deviation of daily rainfall intensity (9.19mm d^{-1}) for all stations). Event class 3 was assigned to dates with the largest rainfall amounts per year that did not fulfil the exceedance criteria. To account for the increasing uncertainty in years where an

outstanding rainfall event (class 1/class 2 event) was missing, the three largest daily rainfall totals of a year were flagged as class 3 events. With this procedure, classification was not bound to inflexible thresholds, but the annual rainfall properties of each station were considered in the classification.

4.2.3 Grouping of the weather stations: Cluster analysis run 1 and 2

A cluster analysis was subsequently used to group the stations into clusters of similar precipitation patterns for known EDB event dates.

Cluster analysis deals with separating data into groups whose properties are not known in advance. In general, prior to the analysis even the correct number of groups into which the data should be distributed is not known. Rather, the aim of cluster analysis is the identification of similarities and differences (expressed as multivariate distances) between individual observations which is used to delineate the groups, and to assign group membership *(Wilks, 2006)*. Cluster analysis can bring out groupings in the data that might otherwise be overlooked, possibly leading to an empirically useful stratification of the data, or help to suggest physical bases for observed structure in the data *(Wilks, 2006)*.

There are numerous examples in the literature that have proven the usefulness of this grouping method in climatic research *(e.g.: Wolter, 1987; Fovell and Fovell, 1993; Guttman, 1993; Unal et al., 2003; Seibert et al., 2007; Toreti et al., 2010)*. A related example is the paper by *(Kalkstein et al., 1987)*, who examined different clustering methods on a temporal synoptic index to group daily weather observations into synoptic types.

The main purpose of the cluster analysis in this study is to derive spatial clusters based on daily rainfall amounts on days with a debris-flood occurrence. As no assumptions on the number of clusters should be made in the first place, we used

hierarchical, agglomerative clustering. We examined three different linkage methods (single, complete, and average linkage) to test whether the groups obtained were stable. Stability was assessed comparing the dendrograms (tree diagrams) resulting from the three different linkage methods.

During the first run, daily precipitation amounts were taken only of the events designated in the EDB and the dendrogeomorphic reconstructions. The purpose of this initial clustering was to identify the structure of precipitation on known event-dates. The second cluster analysis was performed to clarify this grouping, i.e. to get stronger evidence of the covariability of the stations in the case of an extreme rainfall event. For that purpose we only included EDB events from outstanding extremes at all stations and excluded EDB dates with relatively low daily totals.

4.2.4 Seasonality of debris-flood events

Debris-flood season for the catchment had to be defined to exclude extreme precipitation events that occurred in the form of snow.

As the study site itself is not equipped with a weather station, we derived monthly mean temperatures for the weather station with the highest elevation (Hinterriss, 930m a.s.l.) and selected only the months with a mean temperature above 0°C. As the mean elevation of the catchment itself is considerably higher (~1500m a.s.l.) we were sure not to exclude an excessively large part of the data as generally irrelevant.

Nevertheless, in the case of exceptional rainfall amounts outside the seasonal borders, a long temperature record from southern Germany (Hohenpeissenberg, 977m a.s.l., 47° 48` N / 11° 01´ E, 60km from study site) was consulted to determine the gross temperature regime for the days in question.

The importance of the seasonality of debris floods in this catchment, as inferred from the reconstruction, is discussed in more detail in relation to the prevailing synoptical weather situations (see Chapter 4.3).

4.2.5 Visual classification of possible event-dates

Two series of plots were drawn. In the first run, the stations were arranged according to their distance to the catchment before plotting. The second run of plots was produced with the stations arranged according to the second cluster analysis. To account for the possibility of very local occurrence of high magnitude rainfall events, we used cluster analysis only to arrange the stations in the plot, but not to produce plots of mean cluster precipitation.

With the two series of plots, multiple possible event-dates were seeked to be reduced to the most probable event-date per year. For that purpose, the classified event-dates of the ranking classification were marked in the plots. In presence of an extraordinary event, exceeding rainfall totals of 50mm d^{-1} (which is in the range of the mean of all class 2-events), at the station or cluster next to the catchment, this date was flagged a possible event-date. In absence of such an extraordinary event, the date where the marked dates of most stations agreed was identified as the most probable event. In some years, however, the agreement of the stations was too poor to fix a single date. In this case, the three dates with the highest agreement were identified as the most probable events.

The two independently derived sets of probable event-dates (from the two series of plots) were then compared. Dates where the two sets perfectly agreed were assigned a high reconstruction confidence. Single dates that agreed in between the two sets, but came from multiple possible dates, were assigned a moderate reconstruction confidence. If more than one or none of the possible dates between the two sets agreed, the year was flagged with a poor reconstruction confidence.

The entire dataset of probable event-dates with a high or moderate reconstruction confidence (CLASS dates) was consequently used for the evaluation of the classification and the comparison to the EDB dates.

CLASS dates and EDB dates were subsequently used for the next step of the analysis, linking the local precipitation to atmospheric pressure level anomalies.

4.2.6 Evaluation of the classification procedure

To evaluate the classification procedure, two different clustering algorithms were applied on the rainfall records of the CLASS dates. Hierarchical clustering was done first and the resulting dendrogram compared to the initial cluster analysis of the EDB dates.

Additionally, the nonhierarchical K-means cluster algorithm *(see e.g.: Wilks (2006))* was used to group the stations from the CLASS dates. This grouping was also compared to the one from EDB events. The aim was to see if the initial grouping from the EDB events could be reproduced with a nonhierarchical clustering method. The main difference to the hierarchical methods is that the number of groups is given at the beginning of nonhierarchical clustering and that these algorithms allow for a reassignment of observations as the method proceeds *(Wilks, 2006)*.

To get a statistical, 1-dimensional measure of the similarity of the two groups, a two-sided Kolmogorov-Smirnov test on the means of the EDB dates and the CLASS dates was performed.

4.2.7 Thresholds, return levels and trends of extreme precipitation events

Thresholds are by definition the minimum conditions capable of triggering a debris flood *(Guzzetti et al., 2007)*. We examine the applicability of this classical

threshold concept in the case of multiple rainfall stations. In addition, we try to derive thresholds in the form of empirical thresholds by forming classes of daily precipitation in relation to the frequency of past debris flood triggering. The averages of triggering daily rainfall at the stations are used for a comparison to values from the literature.

Return levels of daily precipitation amounts for 5, 10, 25, 50 and 100 years were calculated with an extreme value model (dePOT: declustered Peak Over Threshold model). Associated uncertainties were calculated with the application of the so-called Delta method on the estimated variance-covariance matrix *(Toreti et al., 2010)*. Seasonal trends for the months where extreme rainfall events are concentrated were computed using the Mann-Kendall test for trend significance and the Theil-Sen test to estimate the trend magnitude (slope). Additionally, the rainfall record was analyzed towards the occurrence of extreme events, using logistic regression *(Toreti et al., 2010)*.

4.3 Atmospheric anomalies during extreme precipitation events

A two-step classification procedure based on self-organizing maps and a genetic K-means algorithm produced the centroids of all clusters of 500hPa geopotential height anomalies that occurred during the events in question (± 2 days) *(Toreti et al., 2010)*. As NCEP/NCAR reanalysis data was used to derive the anomalies, only events after 1948 contributed to the formation of the anomaly clusters.

Two maps of composed clusters were used to link the local occurrence of the extreme precipitation events with the large-scale atmospheric circulation patterns in the mid-troposphere (ca. 5.5km height). This pressure level is important for the assessment of prevailing weather conditions as it reflects the mean height of the polar front and hence is suitable to identify ridges and troughs, frontal zones and regions of warm- and cold air advection.

5 Results

5.1 Geomorphic survey

5.1.1 Basic properties

Zones of rapidly changing channel gradient are referred to as knickzones of channel profiles. At convex knickzones, channel gradient suddenly increases. Concave knickzones are found at locations with sudden drastic decreases in channel gradient *(Schlunegger et al., in press)*.

The upper segments of the catchment are dominated by steep to very steep slopes (~ 35 - 65°). Steepness rapidly decreases to ~5° where the tributary stream channels hit the bottom of the valley. Downstream these concave knickzones, alluvial fans have formed in the past. Beneath this prominent transition at around 1250m a.s.l., the ephemeral Gratzentalbach formed a broad alluvial bed. The bed has a length of approximately 800m before it opens up on a forested cone where it merges with the Gerntal.

5.1.2 Transport capacity and debris supply conditions

The subdivision of the catchment (A-C), previously done on the base of differences in bedrock exposure, also has consequences regarding the inferred sediment transport activity in these tributary catchments. Transport activity was derived from the differing sizes of the debris fans at the entering onto the trunk channel (Figure 7). By far the largest fan (~ 4200m^2) formed at the foot of tributary catchment B, followed in size by the fan of catchment A (~1800m^2).

Sediment transport activity in these two tributary catchments is thus inferred to be larger than in tributary catchment C, whose small fans (~250-800m^2) are partly vegetated and undercut by the trunk stream.

Figure 7: Photographs showing the fans on the three different sides (A-C) of the valley.

As observable in the field and on Aerial Photographs (Figure 8), the vegetation cover is lowest in tributary catchment B, where the jointed bedrock slopes are dissected by a close network of headwater bedrock channels. The fraction of debris contributing area that is connected to the channel network, on the total area of this tributary catchment is ~26%. Hence tributary catchment B is classified as transport-limited regarding the supply of sediment to the trunk channel.

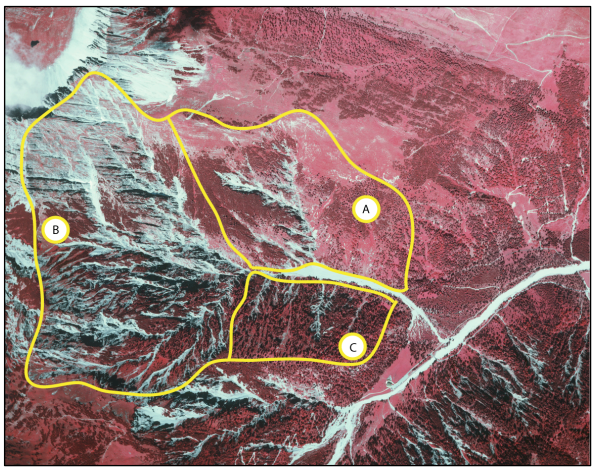

Figure 8: The false-colour near infrared picture illustrates the differences in channel-density and debris-contributing area between the different tributary catchments A, B and C.

Channel density is lower in tributary basin A. However, its western parts towards basin B show extended debris contributing areas with exposed bedrock. The fraction of debris contributing area is ~17% in this tributary catchment. As these parts seem to be well connected to the trunk channel, sediment supply from this tributary catchment to the trunk channel is also subject to a transport-limitation.

In contrast, the channel network of tributary catchment C is much less pronounced. Only a few narrow channels, accounting for ~6% of the tributary catchment's area, connect the continuously vegetated hillslopes with the trunk channel. Thus sediment transport in this catchment is assumed to be supply-limited.

5.1.3 Channel morphology

Figure 9 shows the shaded DEM of the study area with associated steepness indices (k-values) for the four most active channels. Sections in streams 2-4, where the steepness indices reveal a sharp increase (i.e. convex knickzones) are encircled. The concave knickzones are located where these channels hit the alluvial bed of the trunk channel.

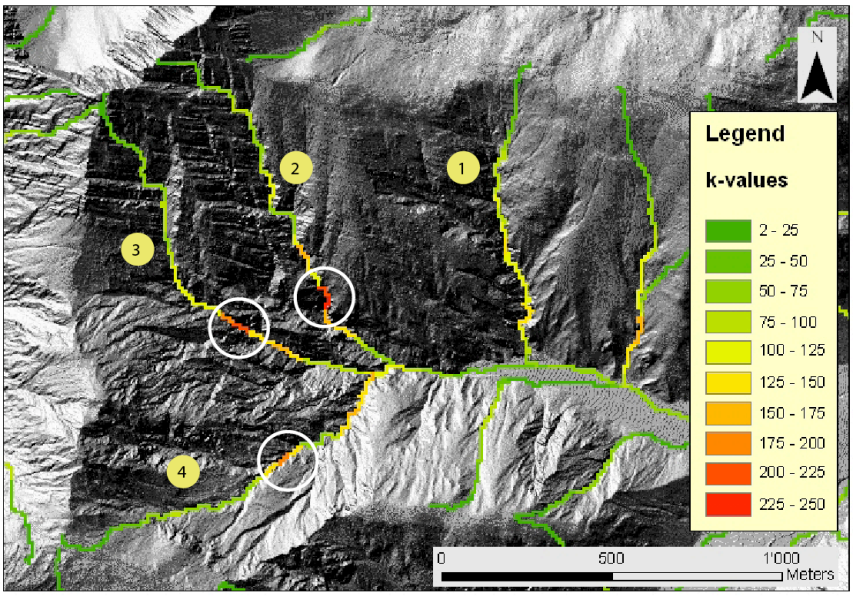

Figure 9: The map shows the k-values (steepness indices, see above) of the four main channels.

The longitudinal channel profiles of streams 2-4 are shown in Figure 10 (left column). All three profiles show, more or less articulately, two knickzones. Arrows indicate the location of the knickzones. The upper knickzone in all profiles is characterized by a sudden increase in steepness (convex knickzone), whereas the lower arrow indicates a knickzone where steepness suddenly decreases (concave knickzone). The convex, less prominent knickzones are located at a level of around 1550m a.s.l. and the concave one at 1250m a.s.l.. While the profiles of channels 2 and 3 plot relatively smooth, the plot of channel profile 4 has a higher roughness. The right column of Figure 10 shows the *log(S)-log(A)* plot for each stream.

Figure 10: The upper row shows the longitudinal channel profiles for channels 2-4. The lower row shows the according log (S) - log (A) plots of the profiles.

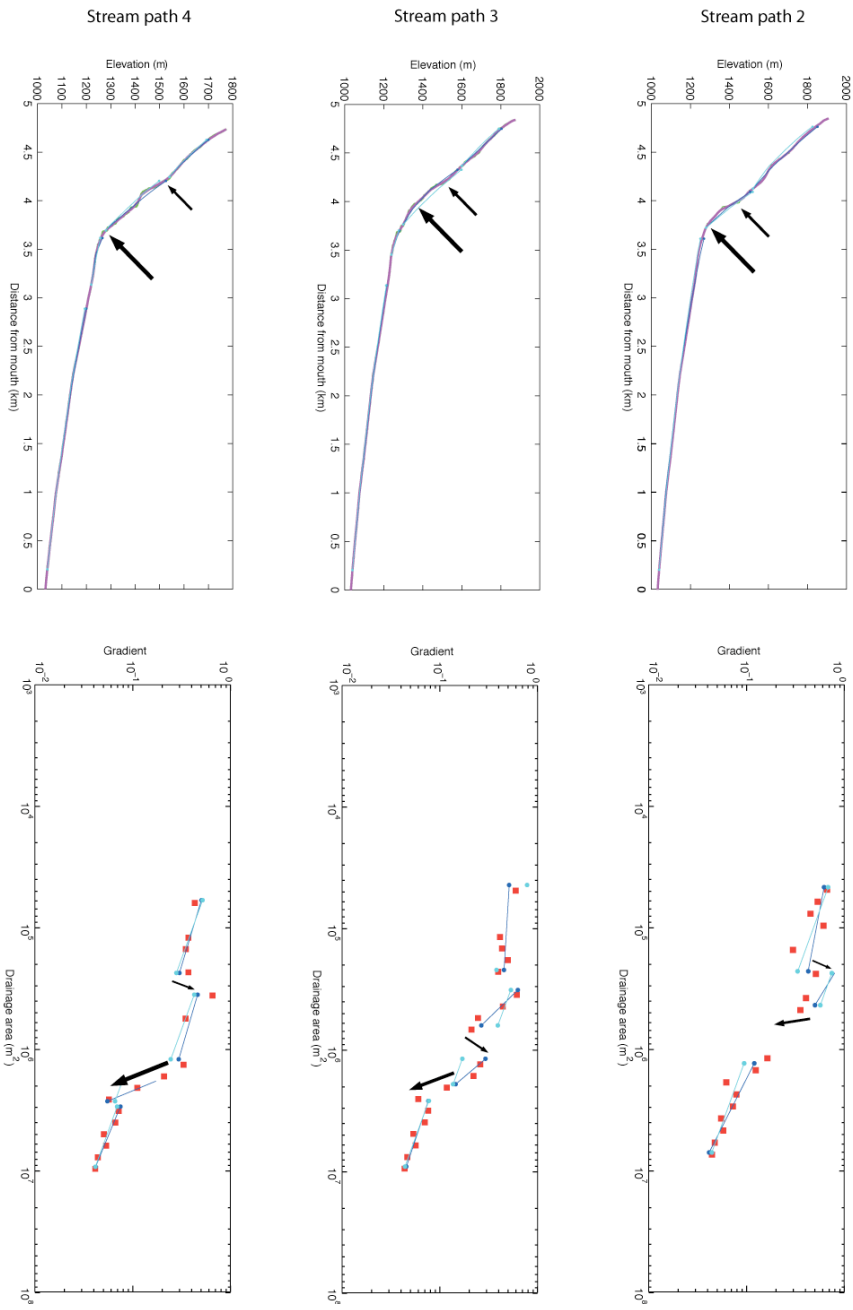

Arrows indicate the position of steps in the logarithmic plots. The plots from channels 2-4 reveal a stepwise increase in channel gradient associated with only a very small increase in drainage area. This step is followed by a larger, more prominent drop, where the gradient reveals a sharp decrease accompanied by a small increase of the drainage area. The second step is followed by a tail of continuously decreasing gradient and increasing drainage area. This shape is found clearest in the plot of stream path 4, whereas in stream path 2 and 3, the steps are not very well discernable.

5.2 Sedimentological field survey

The bedrock channels in the upper parts of the tributary catchments are partially covered with sediment. Large blocks and trunks of trees built up several natural dams between the rock bar at the bottom of tributary catchment B. Right above and beneath the rock bar, deposits of unsorted, matrix-supported debris can be found (Figure 11 a)). At the main knickzone, debris fans of different sizes are apparent.

The largest fan (surface ~4200 m^2) formed at the foot of tributary catchment B. The fan consists of a number of matrix-supported sediment layers (see Figure 11 b)), consisting of a fine, clayey bottom and upper parts of sand and gravel. The layered structure suggests a dominating fluvial sediment transport regime. The large boulders disturbing this structure are deposits of past debris floods. The stream has incised into the fan. The riverbed between the sidewalls of the fan shows a terrassic cross-section with terraces of variable thickness (20-70cm) (see Figure 7 b)).

The fans built of sediments from tributary catchment A are considerably smaller (~1800 m^2). The stream has not incised as deep into the fans as is the case at fan

B. Therefore no information on the inner structure of the fans was available. Several large boulders cover the fan surface.

The fans from unit C show the smallest surface (~250-800 m^2), are partly vegetated, hanging and undercut by the trunk stream.

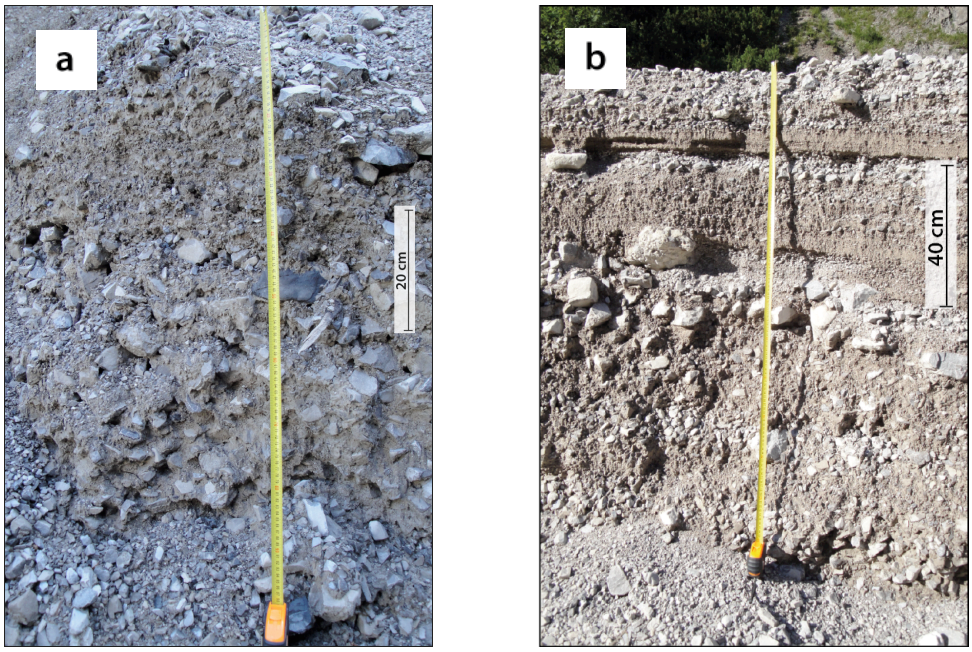

Figure 11: a) Matrix-supported debris at the height of the rock bar. b) Layered deposits at the rear of fan B. Note how large boulders at the left side of the photograph interrupt the layer structure.

Water flowing on the alluvial plane bed of the trunk stream seeps away quickly. With increasing distance from the fans, grain size distribution at the surface changes as the fraction of fine grains rapidly decreases. The dolomitic debris in the trunk stream primarily consists of gravel and sand with a mean grain size of 24.8mm (max. 64 – 256mm). Gravel bars, cross-bedded sheets and lobes with clear bouldery fronts, apparently being depositions of small debris-flood movements from the past *(Strunk, 1995)*, tend to evenly cover large parts of the channel bed (Figure 12a). Different outcrops revealed that the bed is (partially)

underlain by layers of clayey and hence less permeable *(Shepherd, 1989)* material (Figure 12b)).

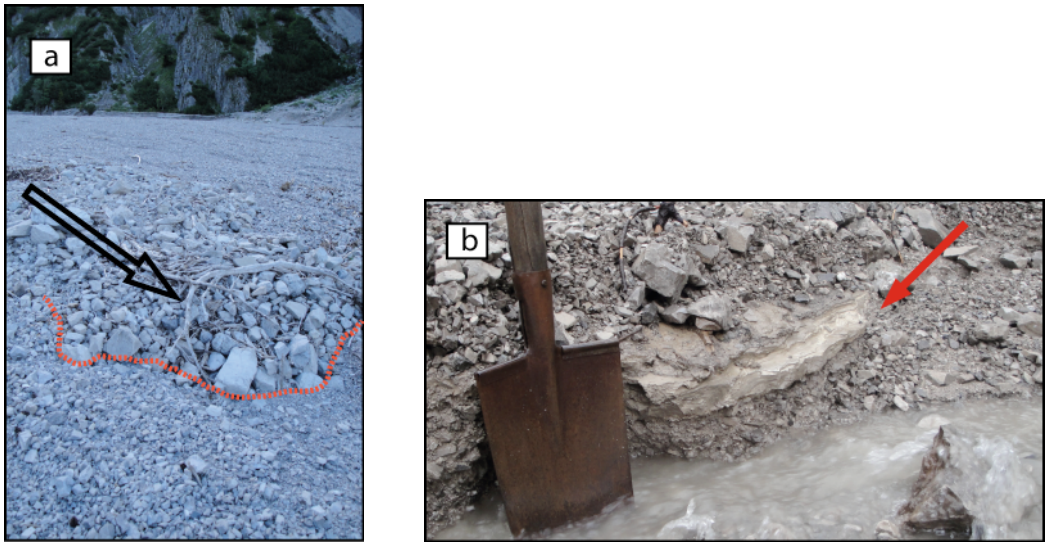

Figure 12 a) A lobe with a clear bouldery front on the plane alluvial bed. The dashed line represents the frontal border of the lobe and the arrow indicates the former direction of movement. b) The clayey layer (red arrow) partly underlying the bed.

The implications of the sedimentologic and geomorphic survey are related to the catchment disposition and the nature of the triggering rainfalls in chapter (6.3).

5.3 Temporal resolution of debris flood records

5.3.1 Characterisation of event-date precipitation

As a first step toward a characterisation of the precipitation amounts for the 5 event-dates known from the EDB, summary statistics were calculated to assess location and spread of the precipitation data.

Thereby the mean and standard deviations of precipitation at the event dates as well as antecedent precipitation up to 5 days were calculated (Figure 13).

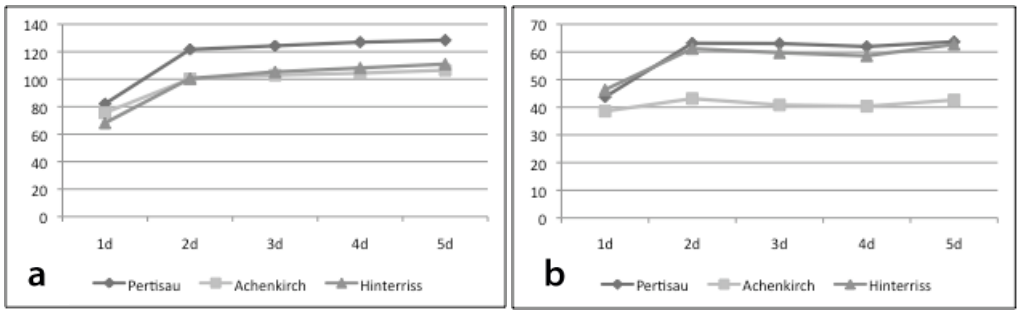

Figure 13: a) Means and b) standard deviations of the reported rainfall amounts [mm] on precipitation events (1d) and the sums of antecedent precipitation (2d – 5d).

Daily means for the precipitation during EDB events (1d) are close for all stations and range from 68mm d^{-1} to 82mm d^{-1}. Two-day sums (2d) are considerably higher for all stations, whereas the addition of further daily sums of antecedent precipitation does not result in a comparable increase in the mean values.

Spread of the daily sums during these dates was high, but of comparable size for the stations Pertisau, Achenkirch and Hinterriss, located at 5.5, 9.6 and 12.5km from the catchment respectively. Standard deviations increased remarkably for 2 of 3 stations as precipitation from the days antecedent to the known events was taken into account.

The precipitation amounts registered during these 5 events show a large spread and increases in means from 1d to 2d sums are within the bounds of associated standard deviations: Therefore we focused on 1d precipitation sums for further analysis. Thus the influence of antecedent precipitation was disregarded in favour of more homogeneity in the data.

5.3.2 Cluster analysis run 1 and 2: Visualisation and grouping

The first cluster analysis displays the station-pattern of rainfall of the EDB events. Input variables are the daily amounts of rainfall of the EDB dates. Figure 14 shows the dendrograms that resulted from the analysis.

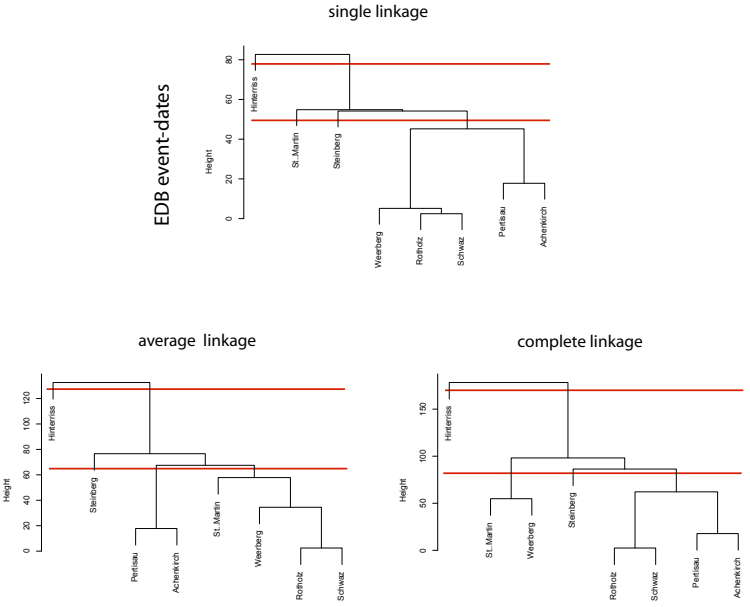

Figure 14: Dendrograms showing the results of the first cluster analysis, processed with known event-dates. Red lines are drawn at two different levels of aggregation (2 clusters / 4 clusters).

The inspection of the dendrograms obtained with single, average and complete linkage of the clusters, revealed different features. The first attribute that is common to all three dendrograms is their step-like shape. This indicates that the distance between the single clusters is relatively small and thus not all the clusters are separated clearly. To compare the three clusters, we chose two possible levels of aggregation. At the first level (lower red line in Figure 14), four clusters could be identified in all plots. Cluster membership of the individual stations varies in between the dendrograms produced with different linkage methods. However, there are stations that were found in the same cluster independent of the linkage method chosen (e.g. Pertisau/Achenkirch or Schwaz/Rotholz). At the second level

of aggregation, only two clusters remain. These are stable in all three dendrograms.

Because the clusters obtained were not separated clearly, especially on a lower level of aggregation, we looked for a possibility to enhance the uniqueness of the grouping. We therefore chose to exclude the events of 1992 and 1995, where the daily rainfall amounts were rather low. Thus the analysis was performed in a three-dimensional space. The result of the second cluster analysis is shown in Figure 15.

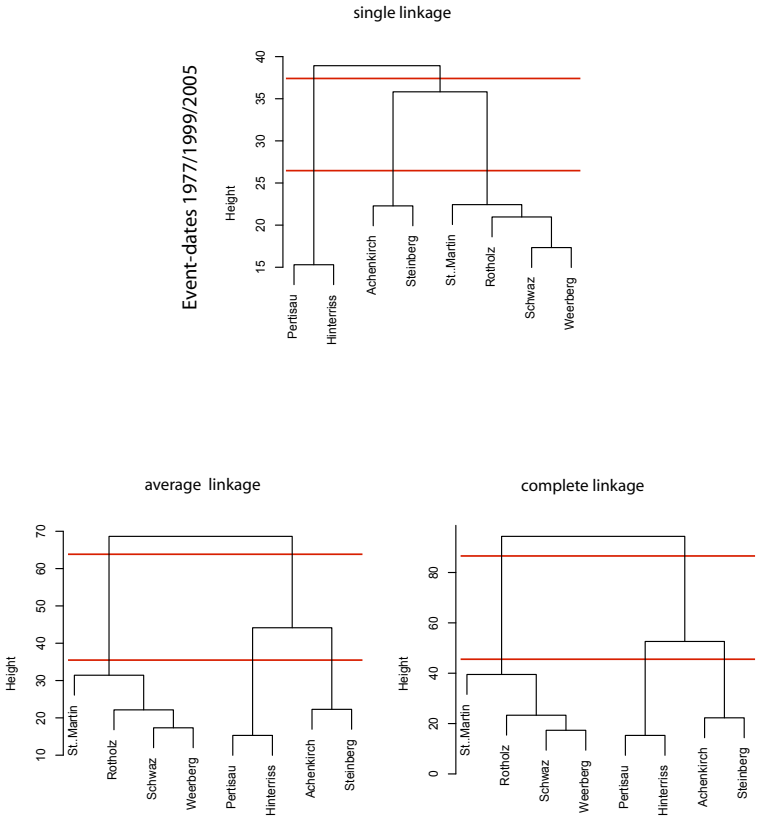

Figure 15: Dendrograms resulting from the cluster analysis with event-date rainfall amounts from years 1977, 1999 and 2005.

The clusters are generally separated by a higher distance than those produced in the first run. On the lower aggregation level, three clusters are persistent over all linkage methods. On the higher level, however, there are differences between the

clusters calculated on the smallest intercluster distance (single linkage) and the other linkage methods. As compared to the previous analysis, these dendrograms display a more distinct grouping of the stations into clusters.

This result changed only marginally when the event year 1912, which was also characterized by a date of outstanding rainfall amounts, was added. Thus we chose to use the three clusters as one type of grouping the stations before plotting the yearly time series of 1d rainfalls.

To meet the concerns that the largest events might dominate the clustering, while events that generally show lower daily rainfall amounts had less weight on cluster formation *(see e.g.: Wilks, 2006)*, we normalized the data by assigning 0 means and unit variance. The inspection of these clusters revealed that they were quite variable regarding the linkage method used (see Appendix). However, the clustering with the average linkage method showed very similar results compared to those from the original data. Consequently we decided to continue the analysis with the original data.

5.3.3 Ranking classification of possible event-dates

The event classes per station and year as a result of the ranking classification are shown in Table 1.

Event year	Pertisau	Achenkirch	Hinterriss	Schwaz	Steinberg am Rofan	Rotholz	St. Martin i.G.	Weerberg
1906	3	3	3	gap	3	3	3	gap
1912	2	2	2	gap	2	2	2	gap
1929	gap	3	gap	3	3	3	gap	2
1934	gap	2	gap	3	2	2	2	3
1938	3	3	3	2	2	2	3	2
1944	2	3	3	3	3	gap	2	3(GP)
1946	2	2	3	gap	3	2	2	3(GP)
1950	2	3	3	3	3	3	3	3
1955	2	2	2	3	2	3	3	3
1961	3	3	3	2	3	2	3	3
1964	2	3	3	3	3	3	2	2
1970	2	2	2	3	2	3	3	3
1973	3	2	2	3	3	3	3	3
1977	1	1	1	1	1	1	1	1
1980	3	3	3	2	3	3	3	2
1983	3	3	3	3	3	3	3	3
1987	3	3	3	3	3	3	3	3
1989	3	3	2	3	3	3	3	3
1992	1	1	1(2)	1(3)	1(3)	1(3)	1(2)	1(3)
1995	1(3)	1(2)	1(3)	1(3)	1(3)	1(3)	1(3)	1(3)
1996	3	2	3	3	2	3	3	3
1998	2	3	3	3	2	3	3	3
1999	1	1	1	1	1	1	1	1
2000	3	3	3	2	3	2	2	2
2004	3	3	2	3	3	3	3	3
2005	1(2)	1(2)	1(2)	1(2)	1(2)	1(2)	1(2)	1(2)
2007	2	3	3	3	3	2	3	3
counts per class								
1	5	5	5	5	5	5	5	5
2	9	7	6	4	7	7	6	5
3	11	15	14	15	15	14	15	15
Summary:								
good / [total]	13/[25]	12/[27]	11/[25]	9/[24]	12/[27]	12/[26]	10/[26]	10/[25]
fraction	0.56	0.44	0.44	0.38	0.44	0.46	0.42	0.40
Exceedances w/o event								
mean class 1	11	3	4	5	6	12	4	16
mean class 2	41	24	18	35	36	19	22	63
mean class 3	289	163	171	220	282	307	221	341
out of records/wet days	16840	19481	18249	13536	18436	16076	16136	14471
fraction	0.00065	0.00015	0.00022	0.00037	0.00033	0.00075	0.00025	0.00111
	0.00243	0.00123	0.00099	0.00259	0.00195	0.00118	0.00136	0.00435
	0.01716	0.00837	0.00937	0.01625	0.01530	0.01910	0.01370	0.02356
Legend:	1(3)	EDB class (Statistical class)						
	3(GP)	Class (gap present in year)						

Table 1: Classification of possible event dates. The entry “gap“ indicates years that were not covered by the respective station records. 1(2) denotes cases where an entry from the EDB would not have entered into the selection by statistical means. 1(3) denotes cases where the entry from the EDB would have had two other competing dates or would not have entered into the selection at all. (GP) indicates that a gap was present in the respective year.

The inspection of Table 1 reveals that there are some dates taken from the EDB that are clearly classified as class 1 events and others whose classification would have been ambiguous without additional information. In summary, the events that were classified with high confidence (class 1 or class 2 events) account for 38-56% of all events (variations between the single stations). This evidence called for

further analysis of the precipitation data, where the accordance of the single events between the stations is additionally taken into account.

The category *exceedances without event* shows the number of days where the station means of a certain class was exceeded but no event occurred according to this classification. The values for the means of class 1 and 2 are remarkably low. Counts for class 3 are already considerably higher. If compared to the number of wet days (i.e. days with daily rainfall amounts ≥ 0.1mm) though, the fraction of exceedances does barely rise above 2.5%. The fraction of exceedances was calculated with the complete records of all wet days, not only with those occurring in event years.

The mean intensity over all stations was 7.92mm d^{-1} with a standard deviation of 9.19mm d^{-1}. Figure 16 shows a boxplot for the mean values of each class and the distribution of rainfall intensities at one of the weather stations.

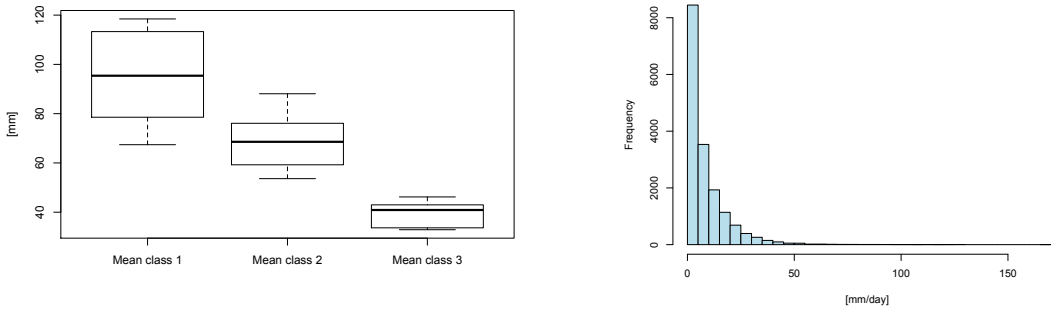

Figure 16: a) Boxplot of the mean intensities of daily rainfall per class. b) Distribution of rainfall intensities at the weather station next to the catchment (Pertisau).

Not only the median but also the spread decreases from class 1 to class 3 events. Means are 95.05mm d^{-1}, 68.69mm d^{-1} and 39.27mm d^{-1} for class 1, 2 and 3, respectively. The histogram illustrates that events with daily rainfall amounts in the range of the three classes occur very rarely.

5.3.4 Visual classification of probable event-dates

Two different series of plots were produced. The first series encompassed the plots where stations are arranged according to their distance from the catchment. For the second series, the stations were arranged according to the groups of the second cluster analysis (run 2).

In both series of yearly plots, the possible event dates from the ranking classification were marked and compared with possible dates from other stations. The decision criterion to fix the most probable date was the following: For extraordinary rainfall events exceeding a minimum of 50 mm d^{-1} (which is close to the lowest station mean of class 2 (53.62mm d^{-1})) at the station or cluster next to the catchment, this event was considered more important than the accordance with the other stations or clusters. In years where extraordinary rainfall events were absent, the dates were flagged as probable event dates where possible event dates from most of the stations agreed. In some cases, however, the agreement was too poor to assign a probable event-date. Figure 17 shows exemplary plots of the three cases mentioned above. The results of the visual event classification are shown in Table 2.

Figure 17: Exemplary plots of run 1 with a probable event-date whose rainfall amounts clearly exceeds the daily rainfall amounts from other days (1955). Event year where the decision for a single event date was based on the accordance of multiple stations (1950) and a year where agreement was too poor to assign a probable event-date (1987).

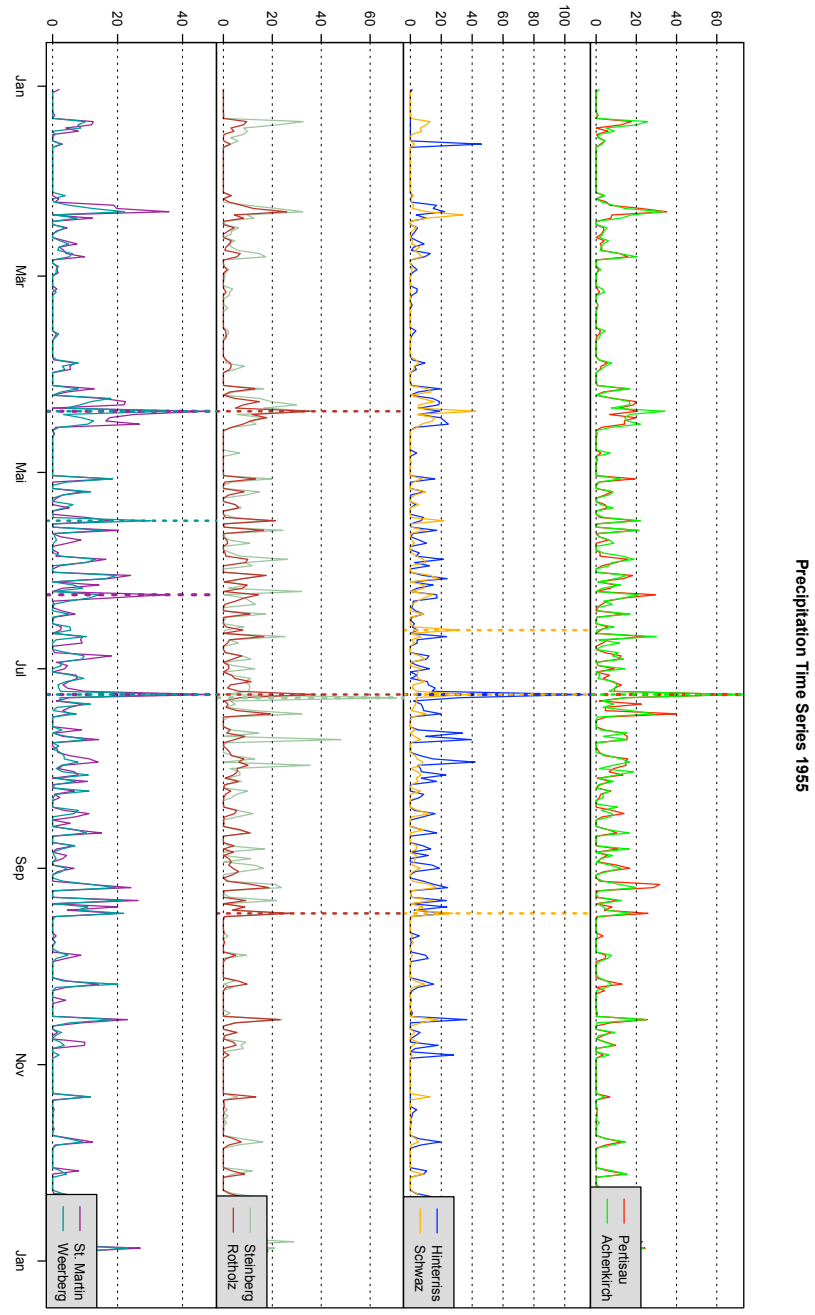

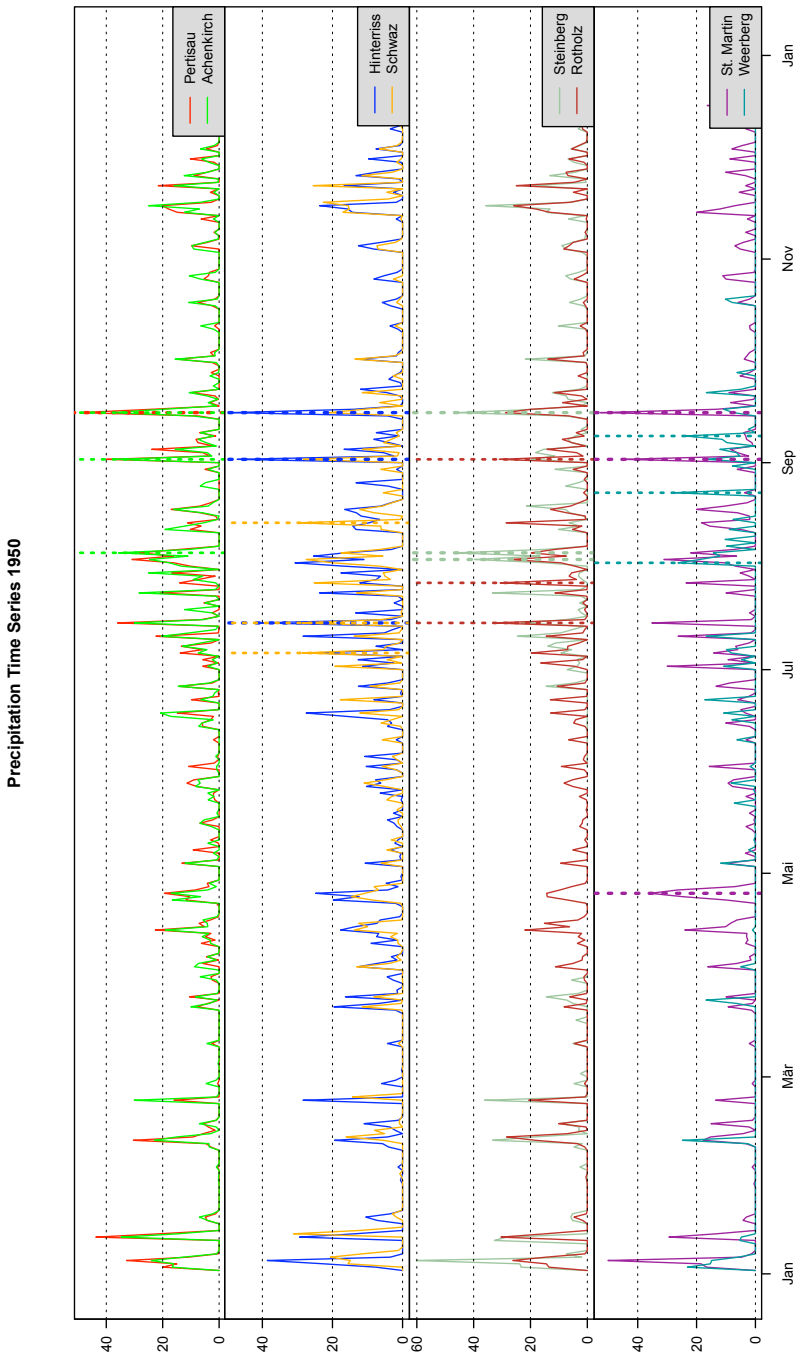
Precipitation Time Series 1950
Pertisau
Achenkirch
Hinterriss
Schwaz
Steinberg
Rotholz
St. Martin
Weerberg
Jan
Mär
Mai
Jul
Sep
Nov
Jan
0
20
40
60

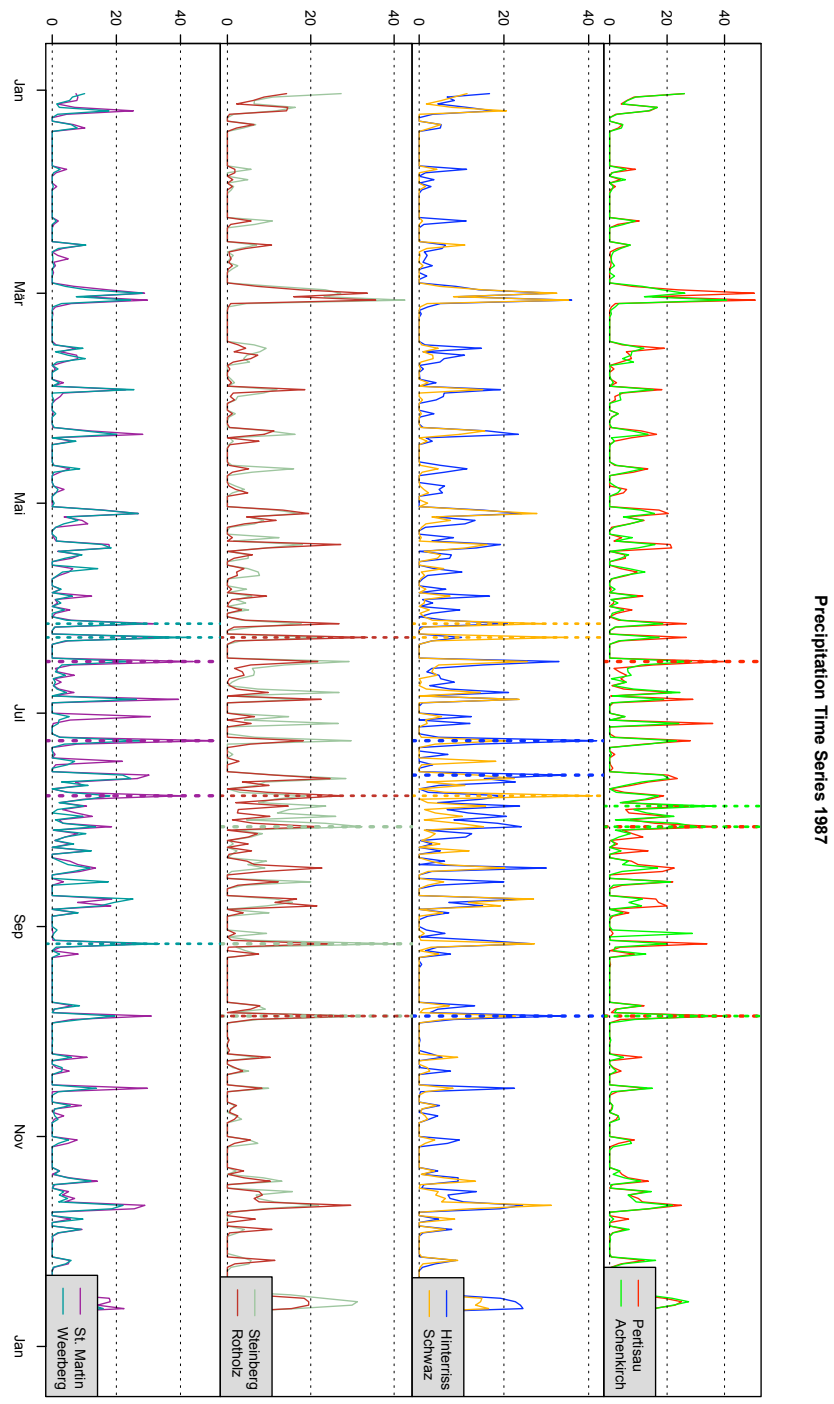
Precipitation Time Series 1987
Pertisau
Achenkirch
Hinterriss
Schwaz
Steinberg
Rotholz
St. Martin
Weerberg
0
20
40
Jan
Mar
Mai
Jul
Sep
Nov
Jan

Year	RUN 1: Distance	RUN 2: Clustered	Confidence level	Station match:
1906	13.7 / 14.7.	?	low	-
1912	8.5.	8.5.	high	(6 / 6)
1929	21.6. / 6.7.	?	low	-
1934	4.8.	4.8.	high	(5 / 6)
1938	27.3. / 28.3.	?	low	-
1944	1.8. / 2.8.	1.8. / 2.8.	low	(4 / 6)
1946	7.7.	7.7.	high	(4 / 6)
1950	1.9. / 15.9.	15.9.	medium	(5 / 8)
1955	8.7.	8.7.	high	(7 / 8)
1961	27.6. / 12.8. / 17.8.	27.6.	medium	(4 / 8)
1964	2.8. / 29.8. / 8.10.	8.10.	medium	(8 / 8)
1970	9.8.	9.8.	high	(7 / 8)
1973	6.7.	6.7. (?)	medium	(2 / 8)
1977	31.7.	31.7.	high	(8 / 8)
1980	23.4. / 3.7. / 20.7.	23.4. / (20.7.)	low	-
1983	13.6. / 14.6. / 29.7.	13.6. / 14.6. / 29.7.	low	-
1987	2.8./15.9.	?	low	-
1989	1.7. / 2.7. / 25.7.	25.7.	medium	(3 / 8)
1992	1.8.	1.8.	high	(6 / 8)
1995	28.8. / 29.8.	28.8.	medium	(5 / 8)
1996	8.7. / (27.5.)	8.7.	high	(6 / 8)
1998	17.9.	17.9.	high	(5 / 8)
1999	21.5.	21.5.	high	(8 / 8)
2000	6.8. / 20.9. / 21.9.	20.9. / 21.9.	low	-
2004	14.8. / 25.8. / 26.8.	? (3.6.)	low	-
2005	22.8.	22.8.	high	(8 / 8)
2007	29.5. / 6.9.	6.9.	medium	(6 / 8)

Table 2: Results of the visual classification.

The table displays the probable event dates, derived for each year from the two runs. While there are often multiple possible events after run 1, the second run narrowed the selection and often resulted in a single probable date. A high level of confidence is assigned to years when both runs showed a perfect match of only one possible date. Multiple possible dates that could be refined to one possible date through the second run were assessed to be dates of medium confidence. When several possible dates were present even after the second run, these years were assigned a low dating confidence. Thus the fraction of events that could be assigned to one probable date (high and medium confidence) is 67% (18 out of 27).

The properties of the event-dates that have been fixed in the course of the analysis are examined in the following. The daily rainfall-amounts of all stations at the dates in question are shown in Figure 18.

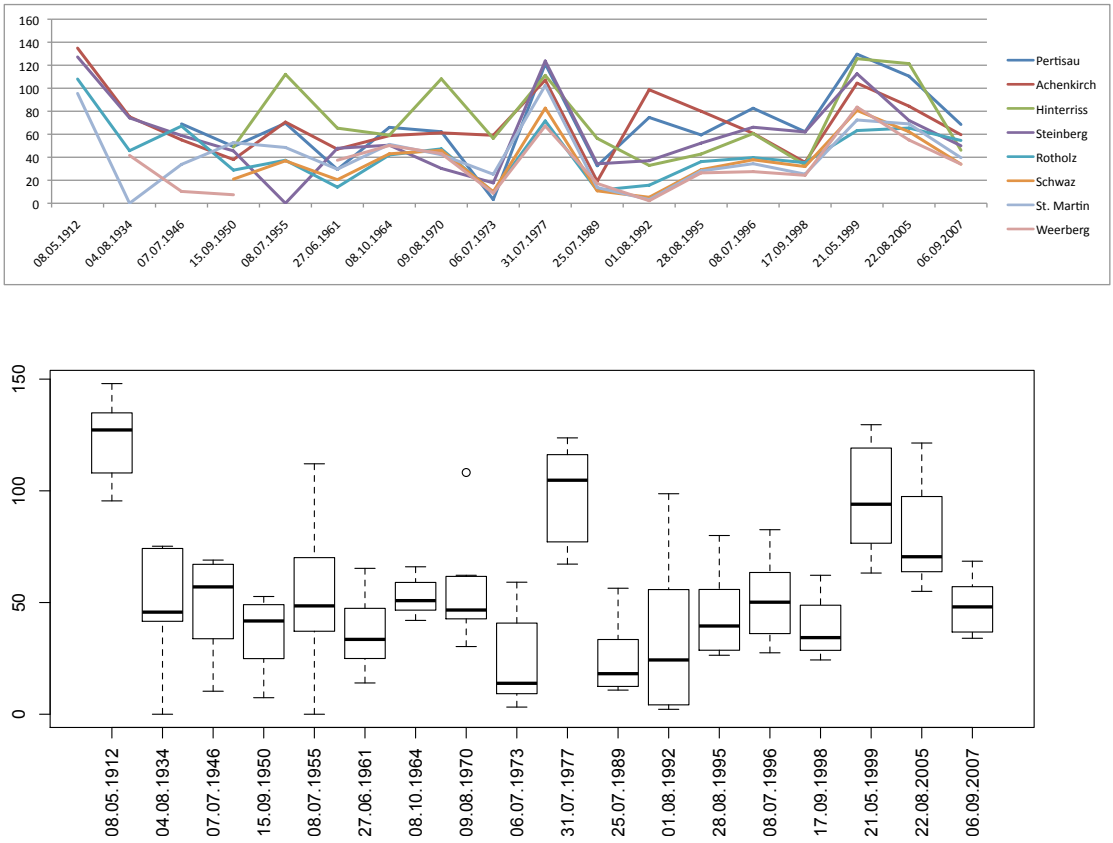

Figure 18: a) Daily rainfall-amounts at all stations on 18 event-dates. b) Boxplot of daily rainfall intensities during reconstructed events for all stations.

Figure 18 a) shows that there is a considerable spread of rainfall amounts at the individual stations. Some stations exceed others significantly at specific event dates (e.g. Hinterriss in 1955, 1970; Achenkirch in 1992). However, this pattern is not uniform over all events. Thus it is inferred that no station predominantly governed the choice of the event dates. The spread of the triggering events, as shown in the boxplot, varies considerably over all event dates. Largest variability is found on the dates when a minority of the stations showed peak values, whereas other stations recorded only small daily rainfall amounts. In general, with very high values of daily rainfall (medians >70mm d^{-1}), the differences in between the stations seems to be higher than at events with more moderate daily rainfalls.

5.3.5 Cluster analysis run 3 and 4: Validation

The 18 event dates that were obtained from the classification above were used as input for the final cluster analysis, which was thus processed in an 18-dimensional space. The resulting dendrograms are shown in Figure 19.

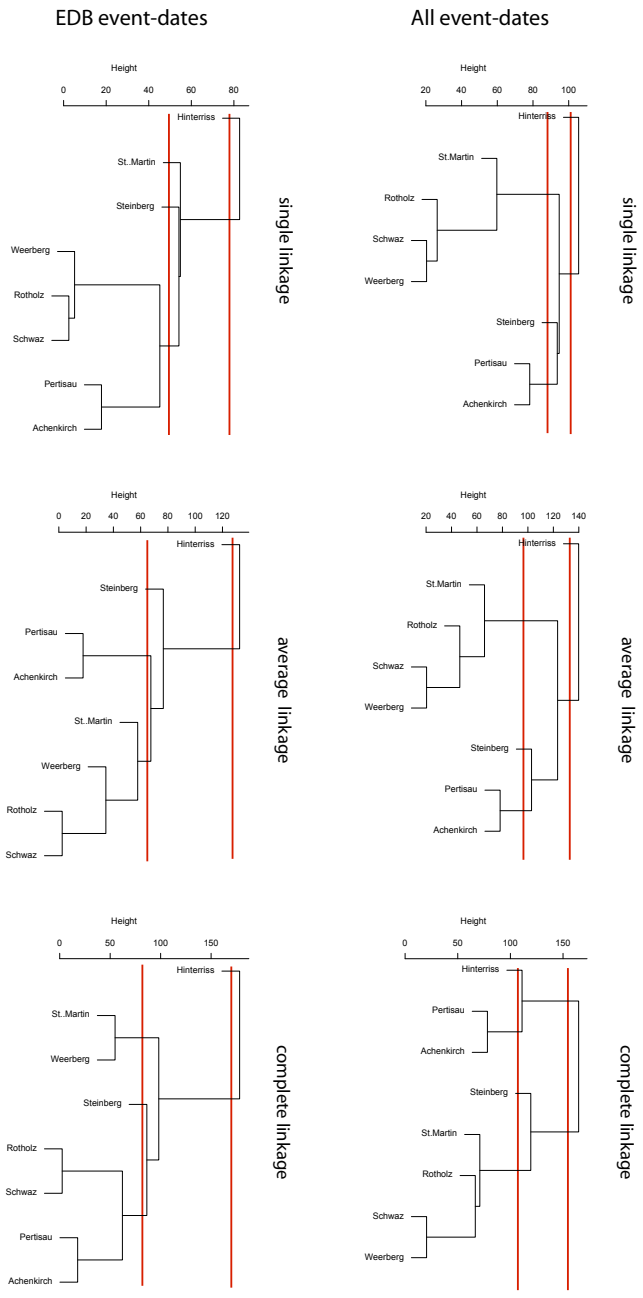

Figure 19: a) Dendrograms obtained from a clustering of all event-dates flagged with high reconstruction confidence. b) Dendrograms that resulted from the first cluster-analysis (EDB dates) are shown for comparison.

The first evidence from the new dendrograms is that a step-shape is also apparent in the results from this run. At the aggregation level of four clusters, however, we find that the four clusters are stable, regardless of the linkage method chosen. At the level of two remaining clusters, the complete linkage version shows some differences to the other two groupings.

When the results of the cluster analysis from all event dates are compared to the EDB event dates, we generally found a good coherence: At the two aggregation levels of two and four clusters, a 100% match of the grouping is obtained with two out of three linkage methods. The best result is obtained with the average linkage method, where a 100% match is observable at both aggregation levels.

The k-means clustering with all event dates, searching for a grouping of 2 and 4 clusters, revealed the results as shown in Table 3.

	Pertisau	Achenkrich	Hinterriss	Steinberg	Rotholz	Schwaz	St.Martin	Weerberg
K=2	1	1	1	2	2	2	2	2
K=4	3	3	4	1	2	2	2	2

Table 3: The cluster membership of the stations, according to the results of the K-means clustering algorithm. K indicates the number of clusters that were formed. The other numbers denominate the cluster that the individual stations were assigned to.

Because the K-means algorithm calculates distances on the basis of vector means (centroids), it is most similar to the average linkage method in hierarchical clustering *(Wilks, 2006)*. Thus it is compared to the results of this clustering method.

At the level of four clusters, the k-means clusters show a 100% match with the results of the hierarchical cluster analysis. However, at the level of two clusters,

there are differences between the results from the two methods: According to the K-means clustering, the smaller group consists of the three stations Hinterriss, Pertisau and Achenkirch, whereas this group only contained the station Hinterriss after hierarchical clustering.

The Kolmogorov-Smirnov test for differences in mean rainfall amounts between the two groups (EDB vs. CLASS) gave a p-value of 0.1826 for a two-sided alternative hypothesis (i.e. the means of the two groups differ significantly). Thus for a significance level above 81.74%, the null hypothesis (EDB dates do have the same mean as the CLASS dates) cannot be rejected.

5.4 Thresholds, return levels and trends of extreme rainfall events

The possibility of threshold definition for the triggering of debris floods critically depends on the variability of the stations under the current setting. The boxplot in Figure 20 shows the variability of event rainfall at the different stations.

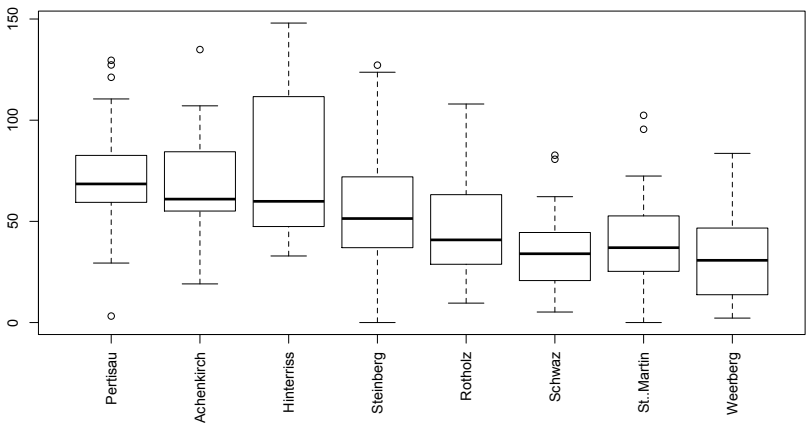

Figure 20: Location and spread of the rainfall events at the level of the individual weather stations.

The stations show a large variability, especially at the stations Hinterriss and Steinberg. Additionally, outliers are present in 5 of 8 stations. The medians of

triggering rainfall amounts (thick black line in the box) decrease with an increasing distance of the stations from the catchment (from left to right, see Figure 4).

5.4.1 Inferring thresholds for debris-flood triggering

Despite the large spread of triggering rainfall amounts, we attempted to derive empirical rainfall thresholds for debris-flood triggering at individual stations. Table 4 shows the share of triggering exceedances of a certain threshold on the total number of exceedances of the same threshold of daily rainfall amounts.

	>60mm	>80mm	>100mm	>120mm
Pertisau	12//84	5//35	4//15	3//7
Achenkirch	10//59	5//18	3//3	1//1
Hinterriss	8//61	6//22	6//10	3//4
Steinberg	7//73	3//24	3//12	2//5
Rotholz	4//31	1//8	1//2	0//0
Schwaz	3//21	2//6	0//1	0//0
St. Martin	4//49	2//8	1//2	0//0
Weerberg	2//44	1//11	0//0	0//0

Table 4: Ratios of triggering-events that exceeded a certain threshold and the sum of all events that exceeded that same threshold.

Generally speaking, the fraction of days triggering a debris flood by exceeding a threshold on the total of days exceeding that same threshold increases with a rise of the threshold. But as a consequence of the high variability, the relative frequency of triggering events does rarely reach feasible height, which is illustrated in Figure 21.

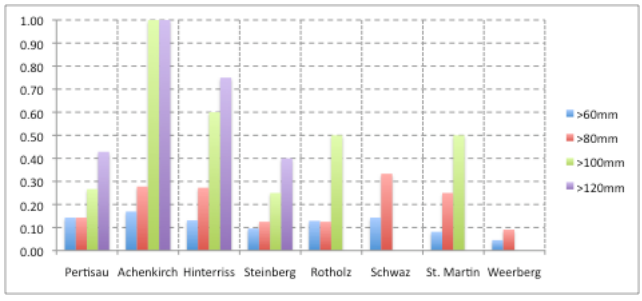

Figure 21: The fraction of events exceeding a certain threshold and thereby triggering a debris flood. Note that only 50% of the stations exceeded rainfall magnitudes of 100mm d^{-1}.

Values of relative frequency (empirical probability) above 50% are attained only on the stations Achenkirch and Hinterriss, when daily totals exceeded 100mm d^{-1}.

The mean of the triggering events of all stations is 55.8mm d^{-1}. The four stations next to the catchment show a mean of 69.2mm d^{-1}, whereas the remaining four stations average to 39.5mm of daily rainfall.

5.4.2 Return levels of extreme precipitation events

Return levels of extreme precipitation, as calculated from the records with the dePOT model *(Toreti et al., 2010)*, are shown in Figure 22. For the calculation of the return levels, the four stations next to the catchment are examined.

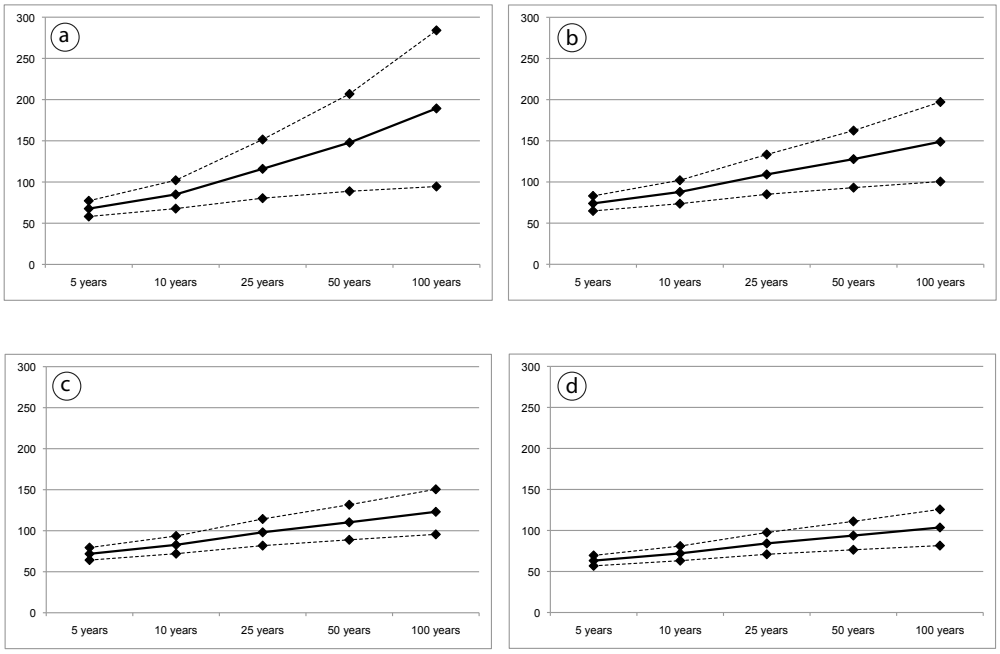

Figure 22: Return levels of extreme precipitation events (solid line) for the stations Achenkirch (a), Hinterriss (b), Pertisau (c) and Steinberg (d) and associated uncertainties (± 1 stdv; dashed line).

Five year return levels are very similar for all stations (~ 67mm d^{-1}). The higher return levels reveal significant differences between the stations. Station Steinberg shows the lowest return levels in total (103.62mm d^{-1} every 100 years), whereas the highest values are found at station Achenkirch (189.28mm d^{-1}). Uncertainty of

the return values increases with the return period and also with the height of the return level.

The maxima of daily rainfall that were recorded at the four stations are 166mm (Pertisau), 150mm (Hinterriss), 140.1mm (Steinberg) and 134.9mm (Achenkirch) since 1895. Where these maxima are within the confidence bounds of a 100yr event for the stations Achenkirch and Hinterriss, they depict cases that have a return period higher than 100 years at stations Pertisau and Hinterriss.

Regarding the return levels of strong precipitation, the 5-year return levels of the stations are close to the mean of class 2-events (68.69mm d^{-1}), whereas class 1 events (mean = 95.05mm d^{-1}) theoretically recur around every 25 years.

The comparison of the reconstructed event dates with dates whose daily rainfall amounts exceeded the 5-year return levels for the four same stations since 1949 is shown in Table 5.

>= 5-yr return level events	Reconstructed dates
12.08.1949	
01.07.1954	
07.07.1954	
08.07.1954	
08.07.1955	
09.07.1955	
13.09.1956	
13.06.1959	
13.08.1961	27.6.
10.06.1965	
11.06.1965	
29.07.1969	
09.08.1970	09.8.
10.07.1972	
01.06.1976	
31.07.1977	31.7.
09.07.1979	
18.07.1981	
19.07.1981	
06.08.1985	
22.07.1992	
01.08.1992	1.8.
28.08.1995	28.8.
08.07.1996	
05.07.1997	
05.09.2001	
11.08.2002	
22.08.2005	22.8.

Table 5: Dates that exceed the return levels at the four stations (Pertisau, Achenkirch, Hinterriss, Steinberg) in comparison to the dates from the classification procedure.

The comparison of the two sets of dates reveals that only 21% of the exceedances triggered a debris flood. However, 5 out of 6 debris flood events coincide with the exceedance of the 5-year return level during an event year.

5.4.3 Seasonality of debris floods and trends of extreme precipitation

Debris-flood season was defined form March to October from temperature records. According to the reconstructions (Figure 23), the debris floods in this catchment occurred from May to October. June and October are the months with the lowest number of events, whereas the peak months are July and August.

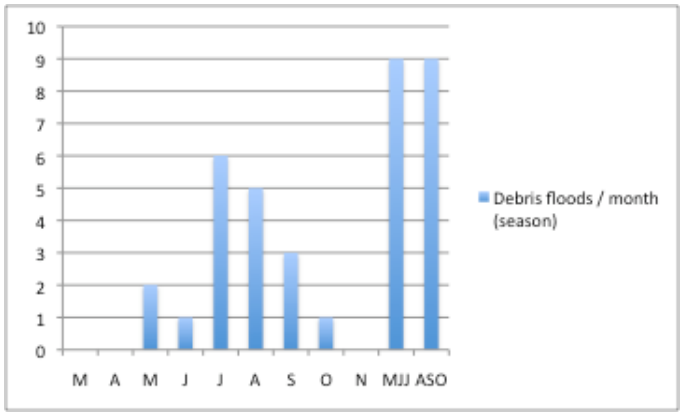

Figure 23: Seasonality of debris floods as inferred from the reconstruction of past events.

The division of the 6 months when debris floods occur in the catchment into parts of early season (MJJ) and late season (ASO) reveals that the cumulative number of debris floods is equal. This distribution is, however, mainly governed by the numbers of the peak months.

As for the trend of seasonal (from June to September) precipitation amounts, only the station Pertisau is characterized by a significant (>90%) positive trend with an estimated slope of 1.9mm yr^{-1} (90% confidence interval: -0.138, 3.726).

Regarding the occurrence of extreme daily rainfall events, none of the station records reveals a significant trend.

5.5 Atmospheric anomalies during extreme precipitation events

The contour maps in Figure 24 show the anomalies of the 500hPa geopotential height field associated with the occurrence of debris floods.

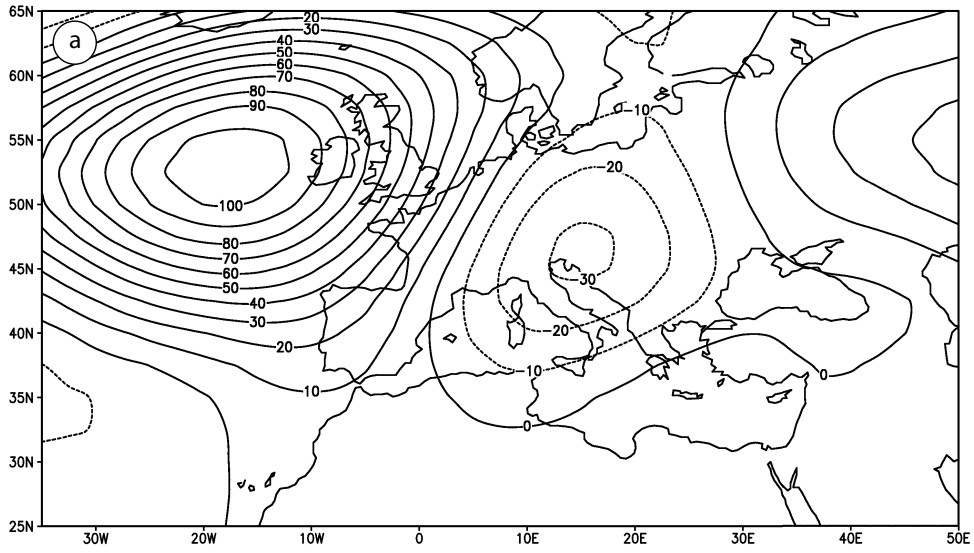

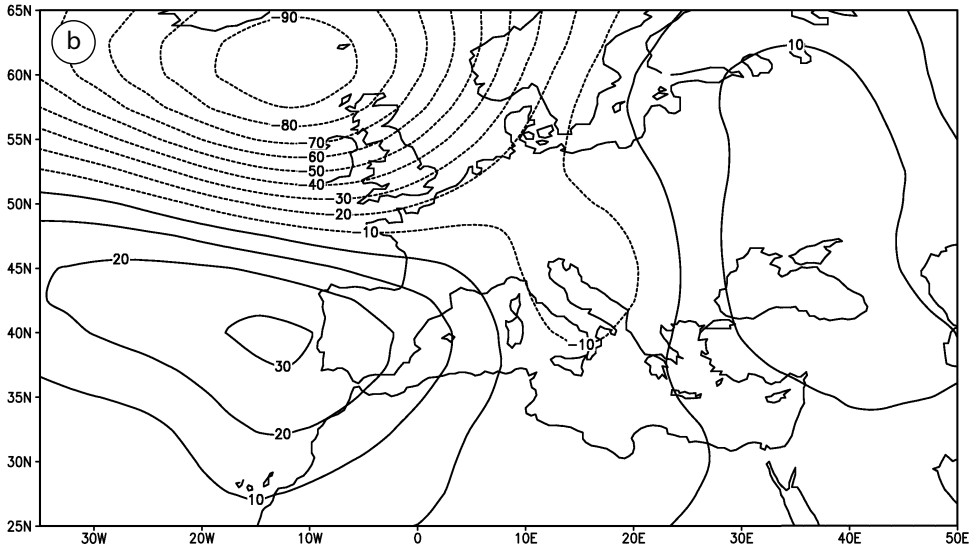

Figure 24: Anomalies of the 500hPa geopotential field height associated with extreme precipitation near the study site. The contour lines are drawn at steps of 10 geopotenial meters (gpm). Solid lines depict regions of positive anomalies, dashed lines show regions characterized by negative anomalies.

Map (a) of 500hPa height anomalies is characterized by a dipole structure, with an axis oriented South-West/North-East. It depicts a high ridge (max. amplitude +100 gpm) centred west of Ireland and a less pronounced trough (min. -30gpm), centred over the North-Eastern Adriatic coast. As the centre of the depression lies further South than the peak of the ridge, the resulting geopotential field over central western Europe is inclined towards Southeast.

The anomaly pattern on map (b) shows a triple centre structure. It depicts a wide ridge, centred offshore the Portuguese coast and a trough extending from the British Isles and Greenland over central Europe, Italy and the Adriatic Sea. More to the East, another slightly lifted geopotential height field covers the regions of Eastern Europe and the Black Sea. Thus gradients are strongest in the eastern North Atlantic, whereas the geopotential height field over Europe experiences only a minor inclination.

6 Discussion

6.1 Geomorphic survey

6.1.1 Basic properties

The geomorphic survey revealed the prominence of very steep (35°-65°) hillslopes connected to a trunk channel with a much smaller inclination (~5°). The length of the trunk stream (600m) and hence the travel distance of debris floods on the channel bed is considerable for this low inclination as past debris floods were reconstructed on the cone at the joining with the Gerntal.

6.1.2 Transport capacity and debris supply conditions

Aerial Photograph analysis of the different tributary catchments revealed that most of the catchment (segments A and B in Figure 8) is subject to a transport-limitation regarding sediment supply to the trunk channel. In accordance to *Bovis and Jakob (1999)* we inferred higher rates of sediment supply from these segments than from the supply-limited, decoupled channels of tributary catchment C. This assumption is in line with previous findings from *Schlunegger et al. (2009)*.

The considerable differences in the size of the fans from the three catchment parts (1800-4200m^2 for segments A and B; 250-800m^2 for segment C) confirms the assumed differences in sediment transport rates. This assumption could, however, be biased by differences in the ages of the particular fans.

On the catchment scale, the debris-flood system was classified as a transport-limited system. Following the conclusions of the work of *Bovis and Jakob (1999)*, this has important implications on the fundamental importance of rainfall as a trigger for debris floods: In transport-limited systems, the frequency of debris floods is mainly controlled by hydroclimatic events.

6.1.3 Channel morphology

In the channel profiles calculated from the DEM (Figure 10), different knickzones were identified. The presence of knickzones in the profiles reveals that the channels are in a transient state where they are not in equilibrium in relation to environmental effects and sediment transport *(Schlunegger et al., (in press))*.

The logarithmic plots of channel gradient (S) versus upstream drainage area (A) were used to identify channel parts that are dominated by fluvial or gravitational sediment transport mechanisms, respectively. The discrimination was not equivocally possible in all profiles. Nevertheless, the upper parts seem to be dominated by gravitational mass moving processes whereas fluvial transport mechanisms prevail in the lower regions.

Thus, debris floods are more effective in transporting sediment in the steep upper parts of the catchment. Debris-flood frequency might probably also be higher on these parts than on the trunk channel, where sediment transport by debris floods only happens during exceptional discharge events.

6.2 Sedimentological field survey

The layered structure of the upper parts of fan B (Figure 11) implies that the deposition of sediment occurred in distinct episodes. The clayey bottom of the layers might present the result of washout processes of the fine-grained matrix

from the surface and a deposition of the solid materials as former rainfalls percolated into the sediments. At several locations, the clear structure is broken by deposits of unsorted, matrix-supported material. These deposits depict the lobes of past debris-flood events that have been preserved in the fan sediments.

The terraces of fan B strongly support the inference of episodic or pulsating water discharge *(Mayer et al., 2010)* and erosional activity. The ephemeral flow of water on the trunk channel might probably incise into the channel at times of high discharge.

The high permeability of the loose sediments in the channel underlines the necessity of extraordinary discharge events so the water flow can be kept at surface level for the entire flow path until the apex of the debris flood cone in the Gerntal. The fact that the riverbed is partly underlain by a layer of fine and hence less permeable material *(Shepherd, 1989)* might be a precondition for the generation of debris floods on such a plane alluvial bed. We assume that water might accumulate on the clayey layers and the water table is then lifted up to the surface level. Consequently, shear strength of the channel material is reduced and hence permits a debris flood to move on with much less friction and without loss of water through seepage. As the water table must be lifted first, rainfall magnitude might possibly play a key role in the formation of debris floods in this type of catchment.

The effect of the trunk stream as a literally unlimited source of sediment is evident. However, for smaller debris-flood events, the long plane bed of loose material could also act as a buffer.

The matrix-free lobes that were found on the alluvial bed are deposits of former debris floods as they are found often in the northern and southern Limestone Alps *(Strunk, 1995)*. A very common process encompasses the secondary reshaping of such deposits by fluvial processes, even if the stream shows an ephemeral flow

regime: The fine materials are washed out of the deposits and often are sedimented on top of the denser, fossil soil horizons, thereby amplifying their inhibitive effect on infiltration *(Strunk, 1995)*.

In summary, the sedimentological survey revealed depositions of past debris floods and deposits form a pulsating flow regime. Additionally, the description of the structure of the alluvial plane bed underlined the extraordinary amounts of water that are a precondition for a large debris flood to persist on the plane alluvial bed of the trunk stream. Of course, the description of these processes remains presumptive as no debris flood could be observed. However, the sedimentary evidence and descriptions of similar processes in the region *(Strunk, 1995)* support this perspective.

6.3 Assessment of catchment disposition to trigger debris floods

6.3.1 Basic disposition

This part of the disposition describes the general susceptibility of a catchment to generate debris flows. The basic disposition depends on the nature of the debris sources, their geotechnical properties as well as the relief. These factors are constant over time or change on timescales from decades to centuries *(Zimmermann, 1997)*.

Debris is readily available and supplied to the trunk channel from the tributary catchments A and B. The trunk channel represents a nearly unlimited source of debris. The geotechnical properties of the debris available vary throughout the channel network in general and also over the length of the trunk stream. A special characteristic is the existence of a matrix in the upper parts of the trunk channel, whereas the deposits downstream lack of fine-grained material. This lack of fine

materials could be a consequence of a longer exposure to washout processes through rainfall more downstream the trunk channel.

The layer of silt and clay that underlies the channel bed is assumed to have a strong influence on the (generally high) local infiltration rates. This might be an important property of the basic disposition.

Overall the steep relief in the upper parts of the catchment favours the formation of debris floods whereas the rather gently inclined trunk channel damps the disposition in total. Thus the basic disposition is assessed as medium (compared to the importance of the variable disposition and the triggering event), especially for large debris floods reaching the debris cone at the end of the trunk channel.

6.3.2 Variable disposition

The variable disposition describes the pre-event conditions or short-term changes in the susceptibility, resulting from hydrometeorological variations on the scale of days to weeks as well as from debris supply conditions based on the torrent history *(Zimmermann, 1997)*.

In this particular catchment, changes in debris supply conditions based on torrent history are not expected to exert significant control on debris-flood frequency. This is due to the nearly unlimited availability of sediment in the trunk stream at the foot of the steep slopes. On the other hand, the variable disposition does not seem to be entirely negligible because water from antecedent rainfalls might be dammed above the less permeable layer in the trunk channel and thus influence the disposition shortly before an event is triggered.

Thus the effect of constant sediment availability is inferred to dominate over the latter factor and the variations of the disposition in the short-term are assessed as being comparatively low.

6.3.3 Triggering event

The system disturbance in the form of a short-term impact is called the triggering event, which ultimately causes the formation of debris flows *(Zimmermann, 1997)*.

According to the previous findings, the triggering hydroclimatic event must be of high magnitude, especially for the generation of large debris floods reaching the cone and affecting tree growth. Relative to the other factors of the system disposition, the triggering rainfall is of utmost importance in this debris flood system. This finding suggests a close link of the precipitation records and the reconstruction of past debris floods at the study site.

6.4 Temporal resolution of debris-flood records

6.4.1 Characterisation of event date precipitation

Using the entries of the EDB to characterize rainfall on event dates, it is important to recognise that the EDB only contains entries on very large and/or recent events. This inference comes from the fact that the population density in the Gerntal is very low. However, the events that affect trees on the cone must also be of considerable size, as mentioned before.

The justification of the choice of 1d rainfall amounts as significant analytic partly comes from the previous findings of an assumed low variable disposition (and thus the small relevance of the soil water status). Additionally, the fact that the standard deviations increased more than mean event rainfalls going from 1d sums to 2d sums (Figure 13) supports that choice. When reviewing the literature, one finds that the periods of antecedent rain considered as being important varies greatly, from days to several months *(Guzzetti et al., 2007)*. Moreover, rainfall

intensities that were derived for long observation periods are averages that might probably underestimate peak intensities *(Guzzetti et al., 2007)*. These findings support the choice of event-day rainfall amounts as the smallest aggregate of precipitation records to start the analysis. However, an additional processing of the analysis with 2d or 3d sums and an examination of possible differences in the outcome could be well worthwhile.

The possible occurrence of multiple events per event year imposed additional uncertainty. Nevertheless, as the fraction of threshold exceedances without an event (see Table 1) is small, the inability of the method to account for multiple events per year is not very serious.

Overall, the characterisation of the rainfall properties of past events provided results that were in line with the expectations from the field survey.

6.4.2 Cluster analysis 1 and 2: Visualisation and grouping

The hierarchical approach proved useful to get an initial grouping of the stations without having to arbitrarily define a number of groups. However, the step-shape in the dendrograms indicates that the individual clusters are not very stable. Because objects that once have been assigned to a cluster remain in that cluster through the whole process, early misclassifications are not corrected for in hierarchical clustering *(Wilks, 2006)*.

The addition of an event year with a very pronounced extreme event in the second run of the cluster analysis might seem somewhat arbitrary. The concerns, that the addition of a high-magnitude event might substantially govern the assignment of groups *(see e.g.: Gong and Richman (1995)*, are appropriate to a certain degree. Yet the only purpose of the second clustering run was to clarify the grouping of the stations in the plots. Hence the results of this run were not included in the

validation of the classification through further runs of clustering or statistical testing. Additionally, the EDB dates were normalized before clustering to eliminate the dominance of single years. However, the results did not change significantly.

6.4.3 Ranking classification of possible event dates

The division of rainfall events on the basis of summary statistics is rather simple, but powerful in the way that it can account for the rainfall characteristics at specific event-years, which were provided by the dendrogeomorphic reconstruction *(Mayer et al., 2010)*. Moreover, as the daily rainfall amount was the criterion selected from the characterisation of past events, the ranking classification was able to account for uncertainty in the case of no outstanding rainfall event.

While assessing the ranking classification, an issue that must be discussed is the existence of dates classified as 1(2) and 1(3) (see Table 1). These are dates that would not have been classified or at least would have been competed by other dates when strictly using the ranking scheme. Yet, these classifications are not evenly distributed over all the stations under consideration. But these cases of apparent misclassifications might have their origin in the characterisation of the EBD dates, or a similarity that does not reach the station records in every possible event year. In most of the cases though, class 3 was assigned and thus given the chance for the agreement of the stations to define the most probable event date.

The reason for the differences of mean rainfall for classes 2 and 3 is obvious, whereas the cause for a higher mean of class 1 remains speculative. A possible answer is that the EDB merely contains the largest events affecting human infrastructure. Smaller events that might not have been registered as destructive

by humans but led to growth disturbances of the trees on the cone thus did probably not enter into the EDB records.

In summary the ranking classification served well as a first step of analysis. An advantage of this classification scheme is that the rainfall properties of the individual stations can be taken into account. At the same time, it showed the limits of the capability of single stations form the regular rain gauge network that has been mentioned by other authors *(e.g.: Strunk (1995); Deganutti et al.(2000))*.

6.4.4 Visual classification of probable event dates

The performance of the visual classification naturally varied in between the event-years. Yet, in numerous cases it was possible to derive an event-date from the accordance of the stations, especially from the plots that were arranged according to the previous cluster analysis (run 2).

When comparing the fraction of events that were designated with a high reconstruction confidence to the station-wise ranking classification, the presumed quality of the reconstruction was upgraded from 38-56% (at single stations) to 67% (after the visual event-classification).

6.4.5 Cluster analysis run 3 and 4: Validation and Interpretation

Comparing the final cluster pattern with the clustering of the EDB dates, the two runs showed a remarkably high agreement of the grouping (e.g. 100% in the case of average linkage at the level of 4 clusters). We thus infer that the event date characteristics from the EDB dates were reasonably well reproduced during the procedure steps of ranking and visual classification. The crosschecking of the grouping with a nonhierarchical clustering method confirmed this perception.

Statistical significance testing in relation to cluster analysis has been done before. *Gong and Richman (1995)* used a pair wise t-test to quantitatively distinguish the performance of different clustering methods. A drawback of the t-test is its parametric nature, assuming a normal distribution of the data *(von Storch and Zwiers, 2003)*. To circumvent this assumption that is likely to be violated with extreme values *(Wilks, 2006)*, we decided to use the Kolmogorov-Smirnov test on the means of the two groups. With the use of this test, the null hypothesis of equal means could not be rejected on the 90% significance level. In either way, the outcomes of this test have to be considered in the context of extreme values. Because extreme values naturally exert a high variability, a significant discrimination of the two groups is challenging. Applying techniques of distribution fitting prior to significance testing with a parametric test could help to improve the power of this test.

The physical meaning of the results of a cluster analysis is an important criteria deciding for the appropriate number of clusters *(Wilks, 2006)*. Hence different spatial implications are discussed in the following. The spatial representation of the cluster run that was most persistent between the different methods is shown in Figure 25.

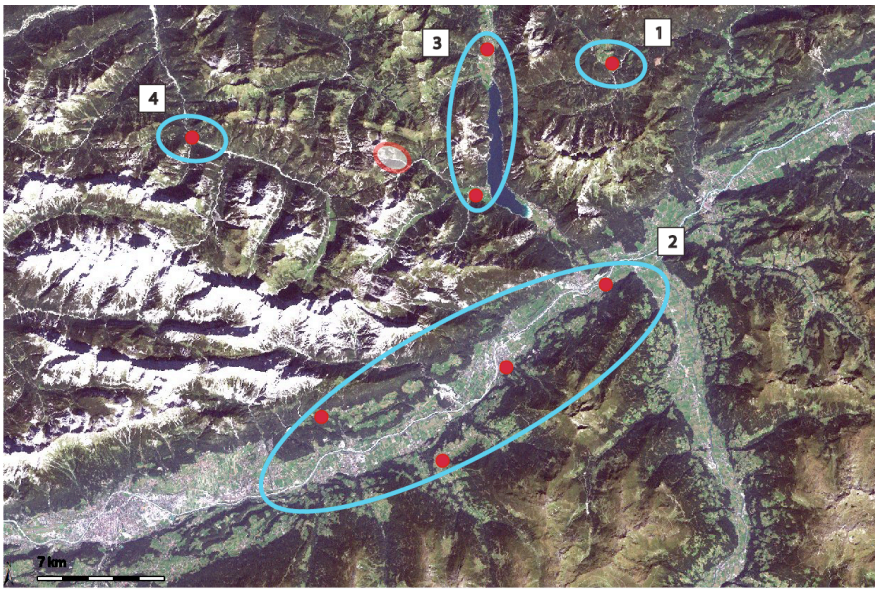

Figure 25: Spatial distribution of the 4 persistent clusters. The numbers refer to the denomination of the clusters in the K-means clustering. The red circle indicates the position of the study area.

The first interpretation relates the clusters to catchment topography. At the level of four distinct clusters, cluster 2 is the largest one. All four stations belonging to this cluster are seated in the Inntal, the E-W-directed main valley of the region. The next smaller cluster 3 is formed by two stations located near the Achensee in a valley that is directed N-S, nearly orthogonal to the Inntal. The station forming cluster 1 is not located in a valley, but on the ridge of a mountain. Cluster 4 lies in a smaller valley that is not directly connected to any of the other valleys.

The relation to the main valley direction where the stations are seated suggests reasonnable implications related to advective rainfall. Thus stations that are situated in the Inntal might preferably react to rainfall approaching from the West, thereby following the main valley. In the case of convective rainfall it is assumed that a convective cell developing in the Inntal preferentially follows the direction of the valley rather than extending to neighbouring valleys.

An interpretation of the clusters regarding station height does not provide reasonable implications. For instance, cluster no.2 comprises stations that range from 535m to 925m a.s.l..

The representation of distance in between the stations is also a possible implication of the clustering, especially when only considering the spatial distribution of cluster 2. But the persistent break to cluster 3 does not imply a clear spatial interpretation.

At the level of two clusters, the differences in group-memberships between the hierarchical and nonhierarchical approach impedes further interpretations. In addition, the spatial inferences are not obvious and would thus remain highly speculative. The results obtained at the level of 4 clusters will hence be the basis for the following discussion relating the local station pattern to large-scale atmospheric anomalies, general weather situations over Europe *(Gerstengarbe and Werner, 1999)* and further related studies *(e.g.: Casty et al. (2007); Seibert et al. (2007))*.

Overall, cluster analysis allowed for a validation of the reconstruction procedure. A statistical test on group means showed no significant differences between known EDB events and reconstructed CLASS events. Even if the single clusters were not separated by large intercluster distances, a stable pattern of four distinct clusters was identified. Finally, the pattern of four clusters allowed for a reasonnable spatial interpretation of the results.

6.5 Thresholds, return levels and trends of extreme precipitation events

The rainfall amounts of all the stations plot with a large spread, even after the selection of specific event dates. This large variability, also being present at the

level of the single stations, makes is difficult to derive reasonable rainfall thresholds for debris-flood triggering at the study site, because thresholds are commonly defined by the smallest event that triggered an event. Thus if the smallest event of any of the stations was taken, a debris flood occurred with no rain recorded (e.g. 0mm d^{-1} at St. Martin in 1934).

Averaging the triggering rainfall amounts from all stations commonly leads to an underestimation of the maxima of daily rainfalls at a specific location *(Guzzetti et al., 2007)*. However, these values allow for a comparison to thresholds form the literature. Table 6 shows different intensity-duration (I-D) relationships for the triggering of debris flows from the literature.

The I-D power law function was initially proposed by *Caine (1980)*. It describes the triggering conditions for debris flows where I is the rainfall intensity [mm h^{-1}] and D is the duration of the triggering rainfall event [h]. To compare the local thresholds from this study to the results from the literature, the triggering conditions for a 24h rainfall period were calculated from the I-D threshold functions.

Source	24h rainfall amount	Spatial scale	I-D threshold function
Present study	55.8mm d^{-1}	Local station mean	-
Present study	69.2mm d^{-1}	4 station mean (min. distance)	-
Present study	39.5mm d^{-1}	4 station mean (max distance)	-
Caine (1980)	102.99mm d^{-1}	Global	$I = 14.82D^{-0.39}$
Zimmermann (1997)	60.99mm d^{-1}	Regional (Alps)	$I = 43D^{-0.89}$
Zimmermann (1997)	51.13 mm d^{-1}	Regional (inneralpine)	$I = 21D^{-0.72}$
Zimmermann (1997)	83.03 mm d^{-1}	Regional (at border of the Alps)	$I = 32D^{-0.70}$
Moser and Hohensinn (1983)	86.53 mm d^{-1}	Regional (Carinthian Alps)	$I = 41.66D^{-0.77}$
Paronuzzi et al. (1998)	228.74mm d^{-1}	Regional (Southern Alpine border)	$I = 47.742D^{-0.507}$

Table 6: Different intensity-duration threshold functions from the literature and the associated triggering 24h rainfall amounts compared to the present study.

With the equation of *Caine (1980)*, hourly rainfall with a magnitude of 14.82mm are sufficient to trigger a debris flood. This was criticized in subsequent studies. *Zimmermann (1997)* proposed the relationship of $I = 43D^{-0.89}$ for the alpine region, $I = 21D^{-0.72}$ for inneralpine regions and $I = 32D^{-0.70}$ for regions at the

border of the Alps. *Moser and Hohensinn (1983)* calculated the relationship $I = 41.66D^{-0.77}$ for the Carinthian Alps in eastern Tyrol. *Paronuzzi et al. (1998)* described the intensity-duration relationship as $I = 47.742D^{0.507}$ for a catchment on the southern border of the Alps.

Figure 26 shows the daily thresholds form this study in comparison to results from other studies.

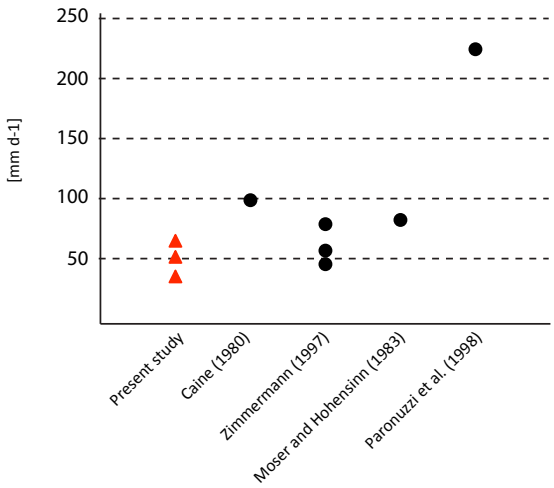

Figure 26: Different 24 hour-thresholds from the literature compared with the values of the present study.

Even if global thresholds generally describe the lower bound of triggering rainfall amounts *(Guzzetti et al., 2007)*, the I-D relationship of *Caine (1980)* delivers high thresholds for the triggering of debris flows. For a rainfall period of 24 hours, the resulting magnitude is 102.99 mm, which clearly exceeds the thresholds calculated in this work. The range of values calculated by *Zimmermann (1997)* stronlgy overlaps our values. The values of *Moser and Hohensinn (1983)* only slightly exceed the maximum value from our catchment. *Paronuzzi et al. (1998)* established an I-D relationship for a catchment at the southern border of the Alps resulting in daily thresholds that are very high. The fact that the return periods in their catchment ranged from 10 to 30 years, whereas the return period in our catchment is ~5.6 years justifies the large differences.

The empirical thresholds allow for the following conclusions: If daily rainfall amounts which are expected to exceed the critical limit of 100mm d^{-1} are forecasted to occur close to the stations Achenkirch and Hinterriss, chances are high (60 - 100%) that these will trigger a debris flood event of measurable size at the study site. However, the high level of uncertainty related to these empirical classes impedes an operational use of these thresholds.

The means of the different classes obtained through the ranking classification can be related to the return levels of daily precipitation. The mean of all class 2 events (68.69mm d^{-1}) corresponds to a return level of ~5 years. Class 1 events (mean: 95.05mm d^{-1}) are related to rainfall events with return periods of 10-25 years. As mentioned earlier, class 1 events are the largest events that occur in the catchment. Thus the high return period of class 1 events seems plausible against this background. The mean return period of events in the Gratzental is ~5.6 years, which is close to the return period of class 2 events.

The comparison of the dates, where daily rainfall amounts exceeded 5-yr return levels, with the event dates that have been defined in this study, reveals a good coherence: 83% of the dates classified in the past conicide with dates that exceeded 5-yr return levels. This result is not surprising, as threshold exceedance was also used to define the single event dates. However, there is not a perfect coherence between these two sets of dates. This is a hint that factors other than daily rainfall amounts influence the triggering of debris floods.

Regarding the trends of extreme precipitation events, the results are coherent with the expectations from the literature *(e.g.: Frei and Schar (2001))*, because the return levels strongly exceed those presently detectable in the rainfall records. The station Pertisau shows a significant trend on the basis of seasonal precipitation. Because the catchment lies in a region with a cool-humid climate, seasonal precipitation amounts are not primarly attained through strong rainfall events.

Thus this seasonal trend cannot clearly be related to extreme precipitation events as done in studies of records from drier climates *(e.g.: Toreti et al. (2010))*.

Regarding the seasonality of debris flood occurrence, the event season found in this work is in line with the seasonal distribution of debris flows from other Alpine catchments. *Zimmermann (1997)* found that the debris flow season for the Swiss Alps ranges from February to November with a peak in July and August. *Andrecs (1995)* found a similar distribution for the Austrian Alps. The shift of seasonality from summer to fall that has been observed in Swiss Alpine catchments *(Stoffel and Beniston, 2006)* and the inference of less frequent but stronger events in the future might possibly also have consequences for the catchment of this study. This assumption is based on the pronounced dependence of debris floods on the pattern and seasonality of extreme precipitation events in the debris-flood system examined.

Summing up, the results were reasonnably well comparable to other studies. In case of the thresholds, the differences could be explained in relation to event frequency. The return levels of daily precipitation amounts corresponded well to the class means form the ranking classification. The fact that there are much more exceedances of the 5yr return levels than debris flood events in the past suggested that, even if the sensitivity of this system to extreme rainfall events is high, there are other factors that significantly influence the triggering of debris floods. The absence of significant trends for extreme precipitation events was in line with expectations from the literature. This finding cannot, however, screen out the presence of trends that are not detectable with the methods and analytics chosen. The seasonal pattern of debris flood occurrence reflects the seasonality of debris flow events in the Central Alps as described by other authors.

6.6 Atmospheric anomalies during extreme precipitation events

In the following, the two maps of geopotential height anomalies are discussed and compared to synoptical studies from the literature.

Generally, fields of positive anomalies of geopotential height arise from warm air with a low density below the 500hPa pressure level. On the other hand, the troughs of negative anomalies are associated with accumulations of cold air masses with a high density *(Malberg, 2002)*. Wind above the planetary boundary layer (PBL, 500-1000m) is approximately geostrophic and its velocity is proportional to the pressure gradient at a given place. Thus high pressure gradients indicate frontal zones of strong winds. Mountain belts can deform frontal zones and lead to a significant disturbance of the geostrophic approximation through increased surface friction and an associated thickening of the PBL. The deflection angle of the wind direction from the geostrophic case is in anticlockwise direction in the northern Hemisphere, averaging about 25° to 35° over land surfaces. This deflection of wind direction (increasing with decreasing height above the ground) as a consequence of frictional effects is referred to as *Ekman-spiral (Barry and Chorley, 1998)*.

The map in Figure 24 a), with a dipole structure of geopotential height anomalies shows a high ridge of warm air centred west of Ireland. The location of the cold air over the northern Adriatic coast in combination with strong inclinations of the pressure field implies the presence of strong NNE winds over Western Europe. More to the east, wind velocities presumably decrease as a consequence of the lower pressure gradient close to the centre of the trough. At lower altitudes, frictional effects force winds to decelerate and wind directions change anti-clockwise. Thus at the level of the PBL, the prevailing wind direction at the location of the study site is estimated to be mainly from North. The inflow of air

towards the low-pressure centre generates upward motion at the top of the PBL, known as *Ekman pumping (Barry and Chorley, 1998)*.

Thus this case might represent an advective situation where air masses are transported toward the Alps form the North. During their passage over the North and the Baltic Sea, they could have humidified. The upward motions in the centre of the low-pressure centre in combination with orographic blocking and lifting of the airmasses at the slopes of the northern Alps might be a plausible implication of this map that is ultimately linked to the occurrence of severe rainfall events at the study site.

Seibert et al. (2007) identified seven synoptic patterns responsible for heavy precipitation in Austria by clustering of airmass-trajectories. Their pattern 5, where the air masses mostly come form a NNW direction highly resembles the situation described in the first map of this study. Additionally, they subdivided the country into regions that are mostly affected by specific patterns. Thus the region comprising the study site is called the "Northern Stau"-region; a region where the most frequent occurrence of heavy precipitation is linked to an orographic blocking of northerly winds. The wind velocities associated with upper and lower level airflow in this pattern also seem compatible with our interpretation of the maps.

The pattern shown in Figure 24 b) with its triple centre structure is dominated by a deep trough of cold air, centred between the British Isles and Greenland. A tongue of rather cold airmasses covers central Europe, Italy and parts of the central Mediterranean and the North African coast. West of the Portuguese coast and in Eastern Europe, rather flat ridges of warm air are situated. In general, the pattern resembles a strong NAO pattern (North-Atlantic Oscillation, see e.g. *Barry and Chorley (1998)*. The topography of the 500hPa pressure level shows the steepest slopes declining from the ridge West of Portugal to the centre of the trough

located north of the British Isles. The convergence of the isohypses more to the West indicates an acceleration of the westerly winds. Once these winds have reached the land surface, they seem to be slowed down due to a divergence to the north of the Western Alps. The deflection of the contour lines toward south implies an advection of negative (anticyclonic) vorticity towards the northern side of the Alps. At the surface level it is assumed that there are only minor wind movements. The subsiding air masses form the higher levels of the Atmosphere lead to atmospheric stabilisation of the warm and moist air masses coming from slow westerly advection. Under this assumedly rather stable synoptic situation, to imagine a situation generating heavy rainfall is challenging. However, the fact that the airmasses presumably have a high humidity and sunny weather conditions are prevailing on the surface level suggest the possibility of the development of strong convective cells. If strong heating is amplified on the higher levels of the mountain slopes, airmasses might be able to shoot up to the cloud condensation level and develop into strong local thunderstorms.

The comparison to the patterns of *Seibert et al. (2007)* reveals highest similarities with pattern 3, denominated North-Western pattern. This pattern is also characterized by lower wind speeds than the other patterns of northwesterly flow. However, a convective component is not mentioned on this pattern.

A comparison of the inferences from the two situations on the maps and the clustering of weather stations around the catchment is speculative, but nevertheless interesting. One could hypothesize that the stations located in the Inntal are more affected by situations that inhibit a stronger westerly flow and a convective component (Figure 24b). The stations outside of the Inntal might show a stronger reaction with situations of orographic blocking of northern flow.

Casty et al. (2007) calculated seasonal empirical orthogonal functions (EOF) of 500hPa geopotential anomalies and related these to changes of surface

temperature and surface precipitation. The pattern from their third EOF (EOF3) strongly resembles our NAO-like pattern of the second map, though with opposite signs. They have shown that this pattern is associated with decreasing trends of surface rainfall. Thus the interpretation of our pattern with opposite signs, delivering high amounts of rainfall in the study area seams reasonable. The trend of decreasing frequency of their summer EOF3 pattern might also have consequences on our opposite pattern.

By means of spatial correlation, *Casty et al. (2007)* confirmed the hypothesis that European precipitation is mainly produced by advective processes in autumn, winter and spring whereas in summer convection plays the dominant role. This is congruent to previous findings by *Wanner et al. (1997*). Thus the debris-flood events at the study site occurred during seasons dominated by convective as well as in seasons dominated by advective weather situations. This further supports the interpretation of our maps.

Both maps from Figure 24 resemble known patterns from general weather situations over Europe *(Gerstengarbe and Werner, 1999)*. The patterns TM (low pressure over central Europe) and TRM (trough over central Europe) whose pressure patterns are most similar to our maps, are both related to higher than normal rainfall amounts.

In summary, the maps of atmospheric anomalies could be related to physical processes of rainfall generation in the Central Alps. Even if a single level of geopotential height anomalies is not able to provide concluding evidence on the total of relevant atmospheric processes, the comparison of these patterns to other studies supported our interpretations.

7 Conclusions

The impact of high-magnitude precipitation events was related to catchment sensitivity and sediment availability in a catchment in the northern Alps. Additionally, the rainfall events were related to the large-scale atmospheric flow by means of Z500 anomalies during debris-flood events.

The assessment of the catchment by the concept of disposition, achieved by means of a field survey and GIS analysis, suggested a need for rainfall events of very high magnitude for the triggering of debris floods in the catchment. A verification of this assessment through detailed observations of an event in the field is desirable. Considering the mean frequency of events in this catchment, however, chances of observing an event are rather low.

The use of different archives of past debris floods allowed an improvement of the temporal resolution of past events. Even though an increase of the temporal resolution from a seasonal to a daily level was possible in many cases, the approach offers a potential for further improvements. Firstly, it is highly desirable to extend the archives of past events in the catchment as these are crucial for the confirmation of the link between debris floods and rainfall characteristics. Secondly, the approach would benefit a lot, when dealing with uncertainty of subjective choices, if probabilistic rather than deterministic statements could be made. This would imply to repeat the analysis based on different choices of relevant parameters (such as the definition of 1d sums as a measure for debris-flood triggering in the system) and for example define dates that have a high probability of triggering an event in the past.

The applicability of station data in the context of debris-flood triggering was examined. The technique of cluster analysis proved useful in grouping event day rainfall patterns and in the validation of the reconstruction of past events. The specification of event years by the dendrogeomorphic reconstruction implied a limitation on the statistical methods available to classify the exact event dates. At the same time, the dendrogeomorphic evidence provided a useful structure for the temporal localisation of past events. The degree of objectivity in this step of the analysis could likewise be increased with multiple choices of relevant criteria (e.g. the thresholds for the ranking classification of the rainfall data). The strong increase in the effort of multiple possible classifications would, however, require a more automated approach. Besides that, interpretations can become very difficult with multiple scenarios and thereby limit the conclusions.

After all, a definition of reasonable rainfall thresholds for the triggering of a debris flood from station data was partly possible in the catchment. Statistically significant trends in the occurrence of extreme events were not found. Nevertheless, there are indications from the seasonality of the events at the Gratzental (summer and autumn) and the literature (increasing trends of extreme precipitation in autumn) that expected future changes in the frequency of extreme events might probably manifest in the debris-flood event frequency in this catchment.

The link of the reconstructed events to the large-scale atmospheric flow showed reasonnable relations to advective as well as to convective precipitation mechanisms. The anomalies of the 500hPa geopotential heights and related synoptical indications for extreme rainfall events were congruent with other findings from the literature. The inclusion of additional height levels might provide further interesting evidence for interpretations of the large-scale atmospheric representations of debris-flood triggering rainfall events.

A last advantage of this approach is its transferrability to other catchments: The adaptation of the analysis to specific catchment characteristics that govern choices of relevant quantities should be relatively straightforward.

Acknowledgements

I would like to thank all the people that contributed and participated in the work of this thesis. Firstly I want to thank Prof. Dr. Schlunegger for the main supervision of this work and all the scientific inputs. I also greatly thank Dr. Markus Stoffel for the co-supervision of this work, his flexibility and his endurance in scientific discussions. Prof. Dr. Jürg Luterbacher is also thanked for the additional co-supervision of the work and for establishing the contact to Andrea Toreti, who I want to express my great thanks to for the calculation of the precipitation return levels, trends and the maps of geopotential height anomalies. Dr. Kevin Norton for the calculation of the river profiles and the stream gradients. Dr. Michelle Bollschweiler for the fruitful discussions and Barbara Mayer for the dendrogeomorphic data.

I also want to express thankfulness to my parents and the rest of my family for supporting me during all these years. I thank Andy for the recreational coffee breaks and all the rest of my friends for the balance they provided during times of hard work.

References

Printed Literature

Andrecs, P., 1995. Einige Aspekte der Murenereignisse in Oesterreich 1972 - 1992. Wildbach- und Lawinenverbau, 59(128): 75-91.

Arattano, M., Deganutti, A.M. and Marchi, L., 1997. Debris flow monitoring activities in an instrumented watershed on the Italian Alps. In: C.L. Chen (Editor), Debris-Flow Hazards Mitigation: Mechanics, Prediction and Assessment, New York, pp. 506-515.

Bagnold, R.A., 1956. THE FLOW OF COHESIONLESS GRAINS IN FLUIDS. Philosophical Transactions of the Royal Society of London Series a-Mathematical and Physical Sciences, 249(964): 235-&.

Barry, R.G. and Chorley, R.J., 1998. Atmosphere, Weather and Climate. Routledge, London / New York.

Bovis, M. and Jakob, M., 1999. The role of debris supply conditions in predicting debris flow activity. Earth Surface Processes and Landforms, 24: 1039-1054.

Caine, N., 1980. THE RAINFALL INTENSITY - DURATION CONTROL OF SHALLOW LANDSLIDES AND DEBRIS FLOWS. Geografiska Annaler Series a-Physical Geography, 62(1-2): 23-27.

Casty, C., Raible, C.C., Stocker, T.F., Wanner, H. and Luterbacher, J., 2007. A European pattern climatology 1766-2000. Climate Dynamics, 29(7-8): 791-805.

Crosta, G.B. and Frattini, P.-. 2003. Distributed modelling of shallow landslides triggered by intense rainfall. Natural Hazards and Earth System Sciences, 3: 81-93.

Crozier, M.J., 1999. Prediction of rainfall-triggered landslides: A test of the antecedent water status model. Earth Surface Processes and Landforms, 24(9): 825-833.

De Baets, S. and Poesen, J., 2010. Empirical models for predicting the erosion-reducing effects of plant roots during concentrated flow erosion. Geomorphology, 118(3-4): 425-432.

De Vita, P. et al., 1998. Rainfall-triggered landslides: a reference list. Environmental Geology, 35(2-3): 219-233.

Deganutti, A.M., Marchi, L. and Arattano, M., 2000. Rainfall and debris-flow occurrence in the Moscardo basin (Italian Alps). Debris-Flow Hazards Mitigation: Mechanics, Prediction, and Assessment: 67-72.

Delgenio, A.D., Lacis, A.A. and Ruedy, R.A., 1991. SIMULATIONS OF THE EFFECT OF A WARMER CLIMATE ON ATMOSPHERIC HUMIDITY. Nature, 351(6325): 382-385.

Flint, J.J., 1974. Stream Gradient as a Function of Order, Magnitude and Discharge. Water Resources Research, 10: 969-973.

Forsttechn. Dienst für Wildbach- und Lawinenverbauung, G.w.U., 2009 a). Pertisauer Wildbäche - Kollaudierungsbericht. (unpubl.).

Forsttechn. Dienst für Wildbach- und Lawinenverbauung, G.w.U., 2009 b). Ereignisdokumentation. (unpubl.).

Fovell, R.G. and Fovell, M.Y.C., 1993. CLIMATE ZONES OF THE CONTERMINOUS UNITED-STATES DEFINED USING CLUSTER-ANALYSIS. Journal of Climate, 6(11): 2103-2135.

Frei, C., Davies, H.C., Gurtz, J. and Schar, C., 2000. Climate dynamics and extreme precipitation and flood events in Central Europe. Integrated Assessment, 1: 281-299.

Frei, C. and Schar, C., 2001. Detection probability of trends in rare events: Theory and application to heavy precipitation in the Alpine region. Journal of Climate, 14(7): 1568-1584.

Frei, C., Schar, C., Luthi, D. and Davies, H.C., 1998. Heavy precipitation processes in a warmer climate. Geophysical Research Letters, 25(9): 1431-1434.

Geol. Bundesanstalt, G., 2008. Zusammenstellung ausgewählter Archivunterlagen der Geologischen Bundesanstalt Nr. 119. In: Geol. Bundesanstalt (Editor).

Gerstengarbe, F.W. and Werner, P.C., 1999. Katalog der Grosswetterlagen Europas (1881-1998). Nach Paul Hess und Helmuth Brezowsky. Potsdam Institute for Climate Impact Research, Potsdam.

Gong, X.F. and Richman, M.B., 1995. ON THE APPLICATION OF CLUSTER-ANALYSIS TO GROWING-SEASON PRECIPITATION DATA IN NORTH-AMERICA EAST OF THE ROCKIES. Journal of Climate, 8(4): 897-931.

Guttman, N.B., 1993. THE USE OF L-MOMENTS IN THE DETERMINATION OF REGIONAL PRECIPITATION CLIMATES. Journal of Climate, 6(12): 2309-2325.

Guzzetti, F., Peruccacci, S., Rossi, M. and Stark, C.P., 2007. Rainfall thresholds for the initiation of landslides in central and southern Europe. Meteorology and Atmospheric Physics, 98(3-4): 239-267.

Guzzetti, F., Peruccacci, S., Rossi, M. and Stark, C.P., 2008. The rainfall intensity-duration control of shallow landslides and debris flows: an update. Landslides, 5(1): 3-17.

Hübl, J. et al., 2002. Hochwasserschutz durch die Reaktivierung von Überflutungsräumen: Evaluierung des Systemverhaltens im Verbauungsprojekt "Pertisauer Wildbäche", Universität für Bodenkultur. Institut für Alpine Naturgefahren und Forstliches Ingenieurwesen, Wien.

Hungr, O., Evans, S.G., Bovis, M.M. and Hutchinson, J.N., 2001. A review of the classification of landslides of the flow type (vol 7, pg 225, 2001). Environmental & Engineering Geoscience, 8(1): 1.

Hungr, O., 2005 Classification and terminology. In: M. Jakob and O. Hungr (Editors), Debris flow Hazards and Related Phenomena. Praxis Publishing Ltd., Chichester UK, pp. 9 - 21.

Hungr, O., McDougall, S. and Bovis, M., 2005. Entrainment of Material by Debris Flows. In: M. Jakob and O. Hungr (Editors), Debris-flow Hazards and Related Phenomena. Praxis Publishing Ltd., Chichester, UK, pp. 135-155.

Hungr, O., McDougall, S. and Bovis, M., 2005 b). Entrainment of material by debris flows. In: M. Jakob and O. Hungr (Editors), Debris flow Hazards and Related Phenomena. Praxis Publishing Ltd., Chichester, UK.

Iverson, R.M., 2000 Landslide triggering by rain infiltration. Water Resources Research, 36(7): 1897-1910.

Iverson, R.M., 2005. Debris-flow mechanics. In: M. Jakob and O. Hungr (Editors), Debris-flow Hazards and Related Phenomena. Praxis Publishing Ltd., Chichester, UK, pp. 105 - 131.

Jakob, M. and Hungr, O., 2005 Introduction, Debris-flow Hazards and Related Phenomena. Praxis Publishing Ltd., Chichester UK, pp. 1-7.

Jomelli, V., Brunstein, D., Grancher, D. and Pech, P., 2007 Is the response of hill slope debris flows to recent climate change univocal? A case study in the Massif des Ecrins (French Alps). Climatic Change, 85: 119-137.

Jomelli, V., Pech, V.P., Chochillon, C. and Brunstein, D., 2004. Geomorphic variations of debris flows and recent climatic change in the French Alps. Climatic Change, 64(1-2): 77-102.

Kalkstein, L.S., Tan, G.R. and Skindlov, J.A., 1987. AN EVALUATION OF 3 CLUSTERING PROCEDURES FOR USE IN SYNOPTIC CLIMATOLOGICAL CLASSIFICATION. Journal of Climate and Applied Meteorology, 26(6): 717-730.

Kalnay, 1996. The NCEP/NCAR 40-year reanalysis project. Bulletin of the American Meteorological Society, 77: 437-470

Kienholz, H., 1995. Gefahrenbeurteilung und -bewertung - auf dem Weg zu einem Gesamtkonzept. Schweiz Z. Forstw., Jg. 146(9): 701-725.

Korup, O., Densmore, A.L. and Schlunegger, F., 2010. The role of landslides in mountain range evolution. Geomorphology, 120(1-2): 77-90.

Luzian, R. (Editor), 2002. Wildbäche und Muren. Eine Wildbachkunde mit einer Übersicht von Schutzmassnahmen der Ära Aulitzky. Bundesamt und Forschungszentrum für Wald, Wien.

Malberg, H., 2002. Meteorologie und Klimatologie. Springer, Berlin.

Mayer, B., Stoffel, M., Bollschweiler, M., Hubl, J. and Rudolf-Miklau, F., 2010. Frequency and spread of debris floods on fans: A dendrogeomorphic case study from a dolomite catchment in the Austrian Alps. Geomorphology, 118(1-2): 199-206.

McArdell, B., Zanuttigh, B., Lamberti, A. and Rickenmann, D., 2003. Systematic comparison of debris-flow laws at the Illgraben torrent, Switzerland. Debris-Flow Hazards Mitigation: Mechanics, Prediction, and Assessment, Vols 1 and 2: 647-657.

Moser, M. and Hohensinn, F., 1983. GEOTECHNICAL ASPECTS OF SOIL SLIPS IN ALPINE REGIONS. Engineering Geology, 19(3): 185-211.

Paronuzzi, P., Coccolo, A. and Garlatti, G., 1998. Eventi meteorici critici e debris flows nei bacini montani del Friuli. L' Acqua, Sezione I/Memorie: 39-50.

Prochaska, A., Santi, P., Higgins, J. and Cannon, S., 2008. A study of methods to estimate debris flow velocity. Landslides, 5(4): 431-444.

Rickenmann, D., Laigle, D., McArdell, B.W. and Hubl, J., 2006. Comparison of 2D debris-flow simulation models with field events. Computational Geosciences, 10(2): 241-264.

Sassa, K. and Wang, G., 2005. Mechanisms of landslide-triggered debris flows: Liquefaction phenomena due to the undrained loading of torrent deposits. In: M. Jakob and O. Hungr (Editors), Debris-flow Hazards and Related Phenomena. Praxis Publishing Ltd., Chichester UK.

Savage, W. and Baum, R., 2005. Instability of steep slopes. In: O. Hungr and M. Jakob (Editors), Debriis flow Hazards and Related Phenomena. Praxis Publishing Ltd., Chichester, UK.

Schlunegger, F. et al., 2009. Limits of sediment transfer in an alpine debris-flow catchment, Illgraben, Switzerland. Quaternary Science Reviews, 28(11-12): 1097-1105.

Schlunegger, F., Norton, K. and Caduff, R., (in press) Hillslope processes in temperate environments. In: M. Stoffel and R. Marston (Editors), Treatise on Geomorphology: Mountain and Hillslope Geomorphology. Elsiever.

Schmidli, J. and Frei, C., 2005. Trends of heavy precipitation and wet and dry spells in Switzerland during the 20th century. International Journal of Climatology, 25(6): 753-771.

Seibert, P., Frank, A. and Formayer, H., 2007 Synoptic and regional patterns of heavy precipitation in Austria. Theoretical and Applied Climatology, 87(1-4): 139-153.

Shepherd, R., G., 1989. Correlations of Permeability and Grain Size. Ground Water, 27(5): 633-638.

Stoffel, M., 2007. Debris-flow activity in the Ritigraben torrent (Valais Alps, Switzerland): Will there be less but bigger events in a future greenhouse climate? Landslides and Climate Change: Challenges and Solutions: 51-58.

Stoffel, M., 2010. Magnitude-frequency relationships of debris flows - A case study based on field surveys and tree-ring records. Geomorphology, 116(1-2): 67-76.

Stoffel, M. and Beniston, M., 2006. On the incidence of debris flows from the early Little Ice Age to a future greenhouse climate: A case study from the Swiss Alps. Geophysical Research Letters, 33(16).

Stoffel, M. and Bollschweiler, M., 2008. Tree-ring analysis in natural hazards research - an overview. Natural Hazards and Earth System Sciences, 8(2): 187-202.

Strunk, H., 1995. Dendrogeomorphologische Methoden zur Ermittlung der Murfrequenz und Beispiele ihrer Anwendung. Theorie und Forschung, Bd. 1, 317. S. Roderer Verlag, Regensburg.

Toreti, A. et al., 2010. Characterisation of extreme winter precipitation in Mediterranean coastal sites and associated anomalous atmospheric circulation patterns. Natural Hazards and Earth System Sciences, 10(5): 1037-1050.

Trenberth, K.E., 1999. Conceptual framework for changes of extremes of the hydrological cycle with climate change. Climatic Change, 42(1): 327-339.

Trenberth, K.E. et al., 2007. Observations: Surface and Atmospheric Climate Change. In: S. Solomon et al. (Editors), Climate Change 2007: The Physical Science Basis. Contribution of Working Group 1 to the Fourth Assessment Report of the Intergovernmental Panel on Climate Change. Cambridge University Press, Cambridge/New York.

Tropeano, D. and Turconi, L., 2003. The October 15, 2000 debris flow in the Bioley torrent, Fenis, Aosta valley, Italy - damage and processes. In: D. Rickenmann and C.L. Chen (Editors), Debris-Flow Hazards Mitigation: Mechanics, Prediciton and Assessment, Davos, Switzerland, pp. 1037-1048.

Unal, Y., Kindap, T. and Karaca, M., 2003. Redefining the climate zones of Turkey using cluster analysis. International Journal of Climatology, 23(9): 1045-1055.

von Storch, H. and Zwiers, F.W., 2003. Statistical Analysis in Climate Research. Cambridge University Press, Cambridge.

Wanner, H., Rickli, R., Salvisberg, E., Schmutz, C. and Schuepp, M., 1997. Global climate change and variability and its influence on Alpine climate - Concepts and observations. Theoretical and Applied Climatology, 58(3-4): 221-243.

Wieczorek, G.F., Coe, J.A. and Godt, J.W., 2003. Remote sensing of rainfall for debris-flow hazard assessment. Debris-Flow Hazards Mitigation: Mechanics, Prediction, and Assessment, Vols 1 and 2: 1257-1268.

Wieczorek, G.F. and Glade, T., 2005 Climatic factors influencing occurrence of debris flows. In: M. Jakob and O. Hungr (Editors), Debris-Flow Hazards and Related Phenomena. Praxis Publishing Ltd., Chichester, UK, pp. 325-362.

Wilks, D.S., 2006. Statistical Methods in the Atmospheric Sciences. International Geophysics Series, 91. Elsiever Inc., Burlington/San Diego/London.

Wolter, K., 1987. THE SOUTHERN OSCILLATION IN SURFACE CIRCULATION AND CLIMATE OVER THE TROPICAL ATLANTIC, EASTERN PACIFIC, AND INDIAN OCEANS AS CAPTURED BY CLUSTER-ANALYSIS. Journal of Climate and Applied Meteorology, 26(4): 540-558.

Zimmermann, M., Mani, P., Gamma, P., 1997. Murganggefahr und Klimaänderung - Ein GIS-basierter Ansatz. Nationales Forschungsprogramm "Klimaänderungen ind Naturkatastrophen" (NFP 31), Schlussbericht. vdf Hochschulverlag AG an der ETH Zürich.

Internet sources

Land Tirol, 2010 "tiris" ; www.tirol.gv.at/tiris, access date14.10.2010.

Appendix

A) Stream profiles

The rate of river incision into bedrock is commonly assumed to be a power-law function of mean bed shear stress, which can be expressed by means of slope, upstream size of the drainage basin, steepness and concavity of a stream profile *(Korup et al., 2010)*. This power-law relationship *(Flint, 1974)* is usually expressed as:

$$S = k_s A^{-\theta}$$

where S is the stream gradient, A is the upstream size of the drainage area and k_s and θ are steepness and concavity indices, respectively.

Because

$$\log(S) = \log(ks) - \theta \log(A),$$

the state of a river profile can be read from a *log(S) – log(A)* plot, where the profile of a graded stream appears as a straight line. Graded longitudinal stream profiles are considered to be in equilibrium in relation to environmental effects

and sediment transport. Genrally speaking, horizontal lines or lines with negative slopes on plots indicate sections of gravity-driven processes, whereas slightly positive slopes on plots indicate fluvial processes. Figure 27 shows three characteristic stream profiles and the according *log(S) – log(A)* plot.

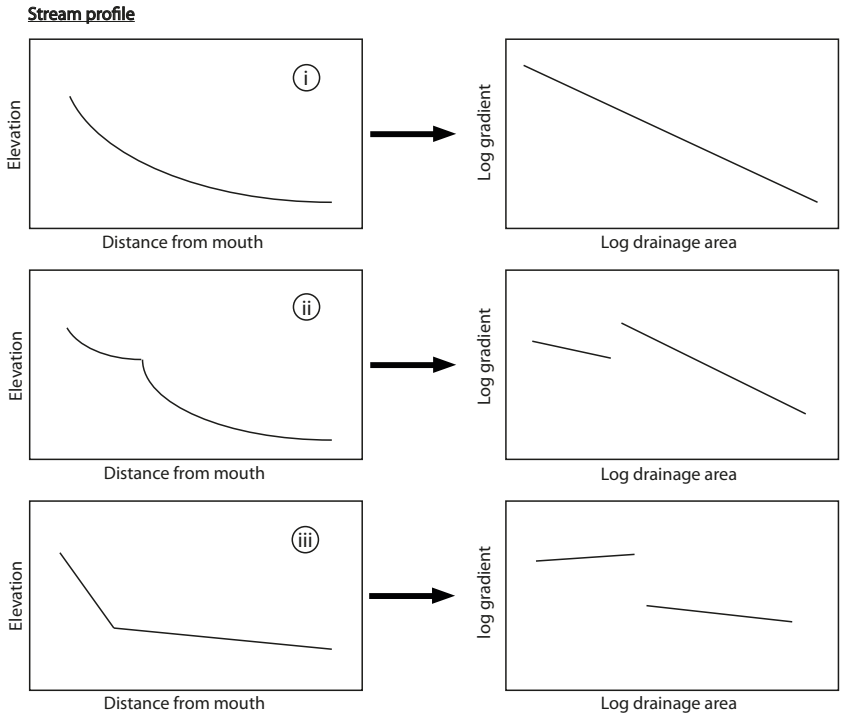

Figure 27: Schematic river profiles and the according schematic log(S)-log(A) plots.

In the uppermost case (i), the river is in equilibrium state and has a balanced stream profile, appearing as straight, decreasing line in the *log (S) – log (A)* plot. In the case of a knickzone, where steepness suddenly increases (ii), an upward directed step indicates the knickzone in the plot on the right. Before and after the plot, fluvial systems are depicted through a line as in case (i). If steepness abruptly decreases (iii), a downward step indicates the knickzone in the *log (S) – log (A)* plot.

B) Clusters of normalized EDB station data

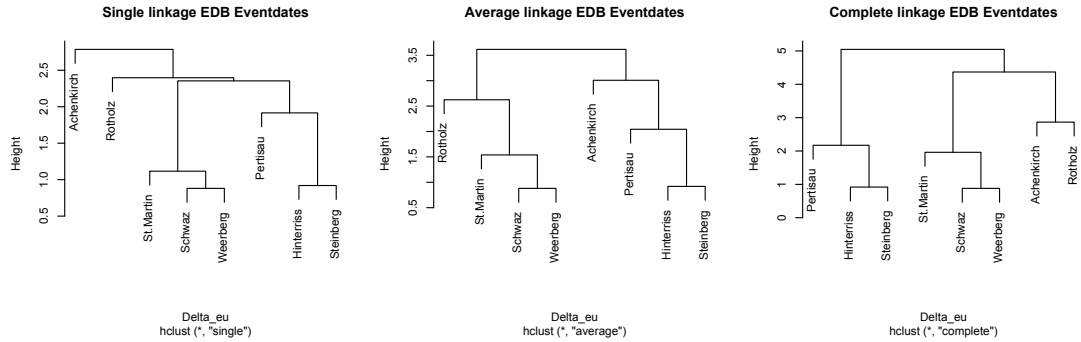

The normalized clusters strongly differred, depending on the linkage method chose. This impeded a clear definition of a cluster pattern. However, the outcome of the average linkage clustering strongly resembled the persistent pattern of clustering run 2 (see Chapter 5.3.2).

C) Process description of debris flows

This chapter introduces into the basic processes and factors related to gravity-induced mass movements and focuses on the conditions that influence the susceptibility for the triggering of debris flows.

Introduction

In general, the term debris flow refers to a process initiated at the toe of landslides, followed by rapid transport of the entrained sediments in a steep channel and deposition of the material on a fan as the slope of the track decreases. Typically, the ratio of liquid and solid parts is rougly equal in volumes, even though this ratio can vary considerably depending on the specific process *(Iverson, 2005)*.

The process generally involves three main stages: The initiation-, transportation- and deposition stage. These are characterized below *(Hungr, 2005)*.

Initiation stage

Sources of debris include nearly any region of unstable and erodible material such as colluvial gully fills, zones of weathered rocks, talus deposits and residual soils. Most often the movement starts as shallow landslides or rock falls that afterwards transform into a debris flow (see below). Sometimes debris flows also develop inside a steep channel by entrainment and destabilization of sediment from the channel bed during situations of extreme water discharge. Initiation of debris flows mostly occurs on steep slopes with dip angles of 20-45°. The limiting factor in flat channels is transport energy. In steep channels, soil cover and sediment availability limit debris flow initiation because feed material is removed during times with regular water discharge *(Hungr, 2005)*.

Transportation stage

Moving debris flows follow trenches that may consist of non-erodible bedrock channels or cascades, channels with erodible soil banks or fully erodible gullies *(Hungr, 2005)*. Often the flow process occurs as distinct surges, which are typically separated by a watery intersurge flow. An event may consist of one or several of these surging waves. In this stage debris flows generally show a typical profile (Figure 28) with a bouldery front that is relatively free of matrix, a main body consisting of a finer-grained mass of liquefied debris, and a tail of turbulent flowing, sediment charged water *(Hungr, 2005)*. Surge fronts are considered to grow large as a consequence of non-uniform frictional resistance that results from the combinated effect of grain size segregation between head and tail, and pore pressure diffusion. Hence the liquefied tail tends to push against the high friction head of the surge, which then can amplify the waveform *(Iverson, 2005)*.

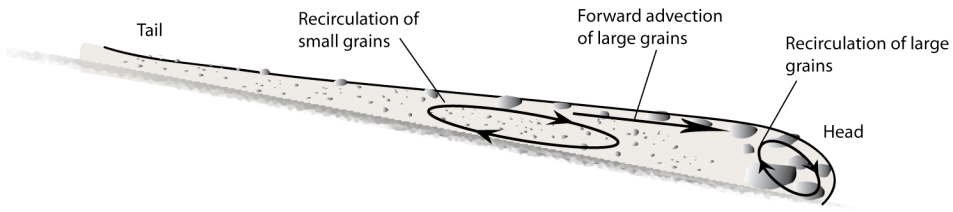

Figure 28: Typical profile of a fully established debris flow. Arrows indicate movement trajectories of different grain size fractions in the surge. Redrawn after (Hungr et al., 2005).

Motion velocities during transport vary greatly, depending on different factors such as steepness, materials involved and type of motion. Velocity determination is crucial for the design of hazard mitigation structures brcause velocity substantially determines the impact forces and runout distances of the movement *(Prochaska et al., 2008)*. Flow velocities can either be measured in the field using e.g. ultrasonic sensors *(Arattano et al., 1997)*, radar and video analysis *(McArdell et al., 2003)*. Alternatively, these can be back-calculated using a so-called super-elevation method *(Tropeano and Turconi, 2003)*. Debris flows have also

successfully been modeled numerically and velocities inferred from these experiments *(e.g. Rickenmann et al., 2006)*. Each of these methods is subject to specific uncertainties. For a more comprehensive overview of applied techniques, see *(Prochaska et al., 2008)*. *Cruden and Varnes (1996)* established a velocity classification for gravity-induced mass movements that typically ranges from *extremely slow* (16mmyr^{-1}) to *extremely rapid* (5ms^{-1}) Although the velocities of debris flows reconstructed with the superelevation method generally lie in the range of 3-15m/s *(Prochaska et al., 2008)*, maximum values as high as 25m/s (Tropeano and Turconi, 2003) to 27m/s (=100km/h!) have been mentioned in the literature *(Luzian, 2002)*.

Deposition stage

Deposition usually happens on a debris fan, sometimes also called debris cone or colluvial fan. Deposition happens as a consequence of slope reduction and a loss of confinement. There are no general guidelines and considerable variation in the literature for the slope angle of debris flow cones. Slope angle delimitation from cones formed by other depositional processes is often not straightforward.

Deposition angles of debris flows are strongly influenced by additional variables. Indeed, observations suggest that with increasing size of debris flows, deposition slope angles typically decrease. Water content also plays a crucial role: Flows with higher water content are usually more erosive and have the lowest deposition angles *(Hungr et al., 2005)*. Other factors that are likely to influence deposition angles are probably existing channel width and -depth, channel bed material, channel bank slope angle and -height, channel bank material and bank slope stability *(Hungr et al., 2005)*.

Material properties often change throughout the fan. At the apex the coarser fractions of the debris material are preferentially deposited. At the distal parts of the fan, the finer and thinner deposits transferred by lower flow velocities are found *(Hungr, 2005)*.

The following chapter discusses the different types of debris flow processes. Subsequently, the process responsible for the transfer of sediment in the study area is specified.

Types of debris flow processes

Stiny (1910) was among the first to recognize that there is no strict distinction between floods and debris flows in steep granular channels, and that the transition from one process to another is continuous. In the course of debris flow formation, the 'normal' sediment transport mechanisms such as saltation and rolling are replaced by a profound instability of the channel bed as the slope angle increases *(Hungr et al., 2005 b))*.

In the past, different attempts to classify flow-like mass wasting processes were made. For example, *Beverage and Culbertson (1964)* created the term *hyperconcentrated flood* to describe the process at the interface between floods and debris flow. *Costa and Jarrett (1981)* made a distinction between *debris flow* and *hyperconcentrated flood* on the basis of the sediment concentration in the flow. *Varnes (1978)* used the grain-size distribution of the material to distinguish between *debris* (soil with more than 20% gravel and coarse sized matter) and *earth* (less than 20% coarse sized material) flows. *Iverson (2005)* made a distinction between flows of highly saturated water and debris flows based on mechanical properties: Whereas the presence of suspended sediment is mostly incidental to the dynamics of the water flow, it is essential for the flow behavior of debris flows. Strong interactions between the solid and liquid constituents are essential for the mechanics of debris flows.

The mass wasting process in the catchment under consideration probably lied somewhere between *debris flows* and *debris floods*. In particular, it was argued that the catchment consists of a steep upper part, where several sediment reservoirs feed a network of supply-limited bedrock channels. The lower part

hosts a broad channel filled with hillslope-derived deposits. Thus in the upper part landslides and debris flows might dominate, while sediment transport in the lower part might probably be accomplished by debris floods.

To highlight the importance of extreme water availability for the formation of mass wasting movements from sources of blocky limestones in general *(Strunk, 1995)* and for this catchment in particular, the mass wasting process in this study area was referred to as *debris flood*, even tough a part of the flow path is in rather gently inclined terrain.

The following section gives an insight into the physics of soil stability and the rheology of debris flows and debris floods.

Mechanical aspects of soil stability and debris flood movement

This chapter outlines the physical and mechanical aspects necessary for the understanding of soil stability and the factors that influence the landslide-triggering of debris flows movement and the down slope sediment entrainment.

Stability of steep slopes

Infinite slope stability models provide a relatively simple approach to the issue of soil stability. They use the principles of static friction operating on a rigid block that rests on a rough inclined plane. Even though the applicability of these models is limited to cases where length and width of a potential landslide greatly exceed its thickness *(Savage and Baum, 2005)*, they are very useful to illustrate the fundamental physics of soil stability. Figure shows the basic essentials of the model.

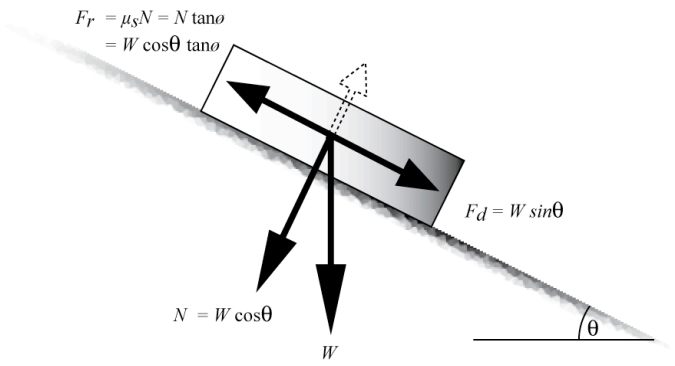

Figure 29: The main forces acting on a rigid block on a rough inclined plane. W is weight or gravitational force, N is normal stress on the failure plane, F_d is driving force and F_r is the resisting force emerging from friction. θ is the inclination angle of the plane, ϕ is the angle of internal friction of the soil and $\mu_{s.}$ is the coefficient of static friction. The dashed arrow shows the force arising by a growth in pore water pressure (see text below). Picture modified after (Savage and Baum, 2005).

The block of soil starts to move as soon as the driving force (F_d) exceeds the resisting force (F_r). Resisting forces depend on the internal angle of friction, the cohesion of the material and the porewater pressure, whereas driving forces are determined through the plane dip angle and the weight of the block *(Savage and Baum, 2005)*. Stress-strain and strength properties of soils can be determined in the laboratory with direct shear and triaxial tests *(Savage and Baum, 2005)*.

Influences on soil stability

This chapter refers to several variable factors that affect soil stability at a given place. It is by no means exhaustive but discusses the most important factors.

Slope dip angle

Slope inclination is one of the most significant mediate factors determining the potential disposition of a hillslope to become unstable under certain conditions *(Moser and Hohensinn, 1983)*. As an intrinsic factor, it directly influences the normal stress on the failure plane and thus the driving force (F_d).

Soil water content

Stress-strain and strength properties of soil combined with the effects of pore water have significant implications for the formation, velocity and travel distance of landslides *(Savage and Baum, 2005)*. Infiltration of water increases the pore water pressure in the soil. In partially saturated and dry soils, a rise in pore water leads to an increase in shear strength due to capillary forces (matric suction) and hence an increase in normal stress *N* and interparticle friction *(Savage and Baum, 2005)*. However, in saturated soils, increasing the pore water pressure reduces normal stress *N* on potential failure planes through the reduction of buoyant weight of the grains and hence reduces the internal friction that resists failure on these planes (see dashed arrow in Figure). For the case of slope parallel seepage where the soil water table coincides with surface level, slopes will fail when the slope angle is approximately half the angle of internal friction for effective stress *(Sassa and Wang, 2005)*. Another effect of increasing soil water content is the increase in weight (*W*) of the whole soil mass and the accordant increase in driving forces (F_d.) Thus water infiltration generally reduces the shear strength of a saturated soil mass *(Savage and Baum, 2005)*.

Seepage plays a key role as sink of water content in soils. The faster water seeps away from the soil, the less water is available for soil destabilization. Seepage is strongly dependent on the hydraulic conductivity of soils and the underlying material. Hydraulic conductivity can range over several orders of magnitude for different geologic materials. Fresh bedrock has a very low hydraulic conductivity, whereas highly fractured and unconsolidated materials are highly permeable. Poorly sorted deposits tend to be less permeable than well sorted ones. Hydraulic heterogeneity and topographic factors strongly influence seepage locally *(Sassa and Wang, 2005)*.

Most important is pososity at the bedrock-soil interface. Bedrock is not part of the soil.

Soil porosity

Another important variable that also has a strong link to soil water content is the porosity of the soil. The reaction of soils to shearing deformation depends on their initial porosity. Loose soils tend to contract under application of normal stress whereas dense soils tend to dilate or expand. Soil contraction in loose soils leads to a reduction in pore volume, an increase in pore water pressure and an accordant reduction of shear strength (see Figure 28). This process takes place rapidly. In contrast the dilating, denser soils tend to react rather gradually. First, they show a dilatant behavior and an increase in pore volume, thereby reducing pore pressure and potentially establishing matric suction. With continuing water supply and a rise in the water table, there is an additional increase of the dilatant behavior or an increase in pore water pressure. The rate at which dilatant behavior happens depends on the hydraulic properties of the soil. The rate is higher in highly permeable soils, whereas it is lower in less permeable soils. Thus contractive, loose soils tend to mobilize faster and have longer runs than dilating, dense soils *(Savage and Baum, 2005)*.

Vegetation cover

Another frequently discussed factor for soil stability is the influence of vegetation and its roots. Landslides in this catchment mostly origin above the tree line. Even though roots of vegetation can act as anchors in the ground and positively influence surface erosion control *(De Baets and Poesen, 2010)* and soil stability, they seldom penetrate deeper than 50cm. Thus their influence is strongest on shallow landslides or on lateral stabilization effects in deep-seated failures. However, root reinforcement may partially control the dimensions of shallow landslides *(Savage and Baum, 2005)*.

Entrainment of material along the flow track

This chapter treats the mechanisms of sediment destabilization and entrainment by a moving debris flow.

It is the efficiency of material entrainment along a debris flow path that determines the final magnitude of a debris flow. The initiating slide is relatively small compared to the large volume of debris that is entrained in the flow along the path. Debris flow magnitude can be described by means of total volume of material moved to the deposition area during an event. Magnitude is an important quantity as is correlates with other parameters such as maximum discharge and runout distances *(Hungr et al., 2005)*.

Water flow on a channel bed destabilizes the bed by drag forces. These are even stronger when the overflowing material is saturated debris instead of water. The mechanisms of destabilization and erosion are sometimes amplified by undrained loading and sliding liquefaction (see Figure) *(Sassa and Wang, 2005)*.

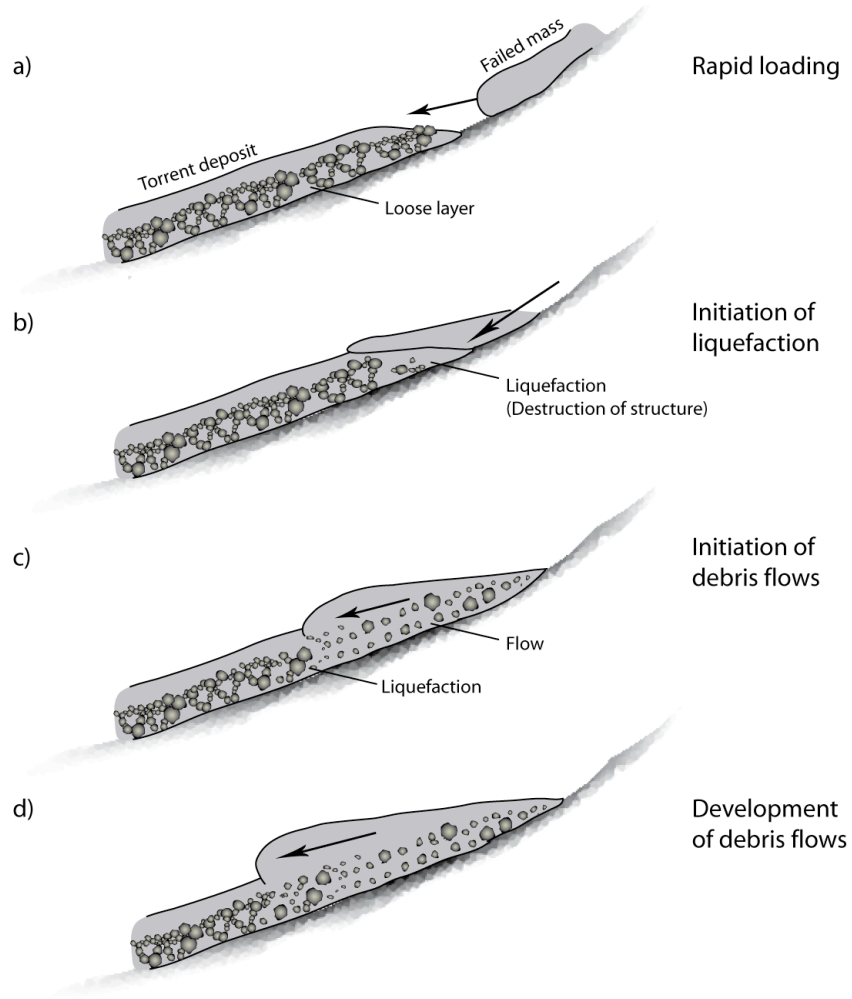

Figure 30: Liquefaction and entrainment of torrent deposits by a moving debris flow. Redrawn after *Sassa and Wang,(2005)*.

Torrent deposits can be liquefied through loading of a sliding mass from the slope above (Figure a)). Under the rapid and therefore undrained loading, the loose structures in the channel debris collapse (Figure b)). The collapse of the structure leads to a reduction in pore volume and thus to an excess in pore water pressure. Thereby the angle of internal friction and thus the resisting force of the underlying soil are reduced (see Figure). As the upper mass now is located on a bed of liquefied torrent deposits, the whole deposit begins to flow and causes liquefactions at its front and an increase in volume of the flowing mass (Figure b) and c)) The liquefaction process can take place in loose, medium or even dense

soils as long as pore volume is reduced by grain crushing under the given overburden pressure *(Sassa and Wang, 2005)*.

In the catchment of this study, entrainment processes play a crucial role as the lower part of the catchment embodies a nearly unlimited source of sediment, which is overran on the way to the debris flood cone. The mechanisms might be a combination of mobilization of debris through extreme water discharges, with an amplification of sediment entrainment by rapid loading and sliding liquefaction of the sediments through the failed mass.

Rheology of debris flow movements

To get an understanding on how a failed mass can reach high velocities and overcome a considerable obstacle such as a long, gently inclined sediment track some basics of debris flow rheology are explained in this short section.

The rheology of debris flows is mainly determined through their behavior as Non-Newtonian fluids. In contrast to fluids of the Newtonian type, Non-Newtonian (or Bingham-type) fluids do not have a constant coefficient of viscosity. The relation between shear stress and strain rate is thus nonlinear. According to the Bingham-model, the fluid behaves as an elastic body until a threshold of shear stress is attained and the fluid begins to flow. Water and solid parts form a homogeneous suspension without segregation and the movement is kept upright through gravity.

For debris flows without a clayey matrix, the Bagnold flow model is appropriate (Bagnold, 1956). In this model, matrix-free flow of water and solid grains is made possible though dispersion pressure of the grains as they move against each other. This model of movement is important for the understanding of debris flows in areas, where debris sources lack of fine-grained material *(Strunk, 1995)*.